"In presenting the dissertation as a partial fulfillment of the requirements for an advanced degree from the Georgia Institute of Technology, I agree that the Library of the Institution shall make it available for inspection and circulation in accordance with its regulations governing materials of this type. I agree that permission to copy from, or to publish from, this dissertation may be granted by the professor under whose direction it was written, or, in his absence, by the dean of the Graduate Division when such copying or publication is solely for scholarly purposes and does not involve potential financial gain. It is understood that any copying from, or publication of, this dissertation which involves potential financial gain will not be allowed without written permission.

_____

_____

THE ANALYSIS OF WING LOADS IN ROLLER COASTER MANEUVERS

A THESIS

Presented to

the Faculty of the Graduate Division

by

Pembroke Graves Rees

In Partial Fulfillment

of the Requirements for the Degree

Master of Science in Aeronautical Engineering

Georgia Institute of Technology

June, 1962

3 6
12 R

THE ANALYSIS OF WING LOADS IN ROLLER COASTER MANEUVERS

Approved:

Arnold L. Ducoffe, Co-Chairman

Frank M. White, Jr., Co-Chairman

Thomas W. Jackson,

Date Approved by Chairman 25 May, 1962

ACKNOWLEDGEMENTS

The author wishes to express his thanks to Professor James A. Stricklin for his suggesting the topic of this investigation. He also expresses his thanks to Dr. Arnold L. Ducoffe, Professor Stricklin, Dr. Frank White and Dr. Thomas W. Jackson for their review of the work.

He extends most sincere appreciation to the Lockheed-Georgia Company for permission to use the technical data on which this investigation is based, and to Mr. C. N. Sanford who helped in many ways.

TABLE OF CONTENTS

LIST OF ILLUSTRATIONS

List of Figures - continued

LIST OF SYMBOLS

A. C.	Aerodynamic center
b	Wing span
c	Wing chord
$\bar{c}$	Mean aerodynamic chord
$\bar{c}/4$	Quarter-chord point on $\bar{c}$
c. g.	Center of gravity
C_L	Lift coefficient, normal to relative wind
$\mathcal{L}$	Centerline
C_m	Pitching moment coefficient
C_{N_A}	Airplane normal force coefficient
C_P	Power coefficient
C_T	Coefficient of thrust
C_z	Vertical force coefficient normal to airplane reference axis
D	Propeller diameter
F.A.T	Free air temperature
F_p	Propeller thrust, lb.
fps	Feet per second
HP	Horsepower
J	Advance ratio
L	Load (general; - S, M or T)
$L_{n=o}$	Zero-g air load
ℓ_t	Tail length: distance from A.C. to $(\bar{c}/4)_t$

List of Symbols - continued

M	Moment, generally vertical bending moment - M_x on the wing, M_y on the nacelles
n	Load factor, the ratio of the inertial force to the force due to gravity
n	Propeller revolutions per second
PSF	Pounds per square foot
P_z	Propeller vertical force
q	Dynamic pressure
r	Radius of propeller
S	Vertical shear outboard of a given wing station or forward of a nacelle station
S	Wing area
SHP	Shaft horsepower
T	Propeller torque
T	Wing torsion about a given y-axis
THP	Thrust horsepower
T_c	Thrust coefficient
t	Time
V	Velocity
W	Airplane gross weight
WS	Wing station: inches from airplane $\mathcal{L}$ along y-axis
B_1, M_1, M_2	Constants from reference 13
N_1, N_2	Constants from reference 13
X	Distance in x-direction from the A.C. to the c.g.
x,y,z	Airplane axes
α	Angle of attack
$\dot{\alpha}$	Time rate of change of angle of attack

List of symbols - continued

Δ	Incremental
$\frac{\Delta L}{\Delta n}$	Incremental load for $\Delta n = 1.0$
$\frac{\Delta L}{\Delta n W}$	Unit additional air load
$\dot{\theta}$	Pitching velocity
$\ddot{\theta}$	Pitching acceleration
ρ_o	Air density at sea level, slugs per cubic foot
σ	Ratio of density of air at altitude to ρ_o
◒	Center of gravity

Subscripts

A	Airplane
a-t	Airplane less horizontal tail
ad	Additional air load
avg	Average
e	Equivalent
f	Fuselage
FRL	Fuselage reference line (horizontal reference line for airplane)
N	Nacelle
p	Propeller
s	Stall
ss	Slipstream
t	Horizontal tail
T	True
w	Wing

LIST OF TABLES

SUMMARY

The purpose of this investigation is the determination of the effect of certain parameters on wing loads in symmetrical maneuvers in order to improve the accuracy of wing loads reduced from flight data. The parameters considered are speed, power, angle of attack, rate of change of angle of attack, pitching velocity, pitching acceleration, and flutter.

The effect of these parameters was investigated on loads recorded by strain gages during a series of push-pull, or roller coaster, maneuvers performed throughout a considerable speed range at a constant altitude by a Lockheed C-130B airplane. The investigation consisted of determining the effect of each parameter then examining the test data to find the magnitude of each effect. Propeller loads for the test conditions were calculated from wind tunnel data. The effects of the other variables were described on the basis of previous knowledge. The test data were examined to determine the magnitude of each effect on the total load versus load factor and on the zero-g and additional air loads. The accuracy of the "slope-intercept" method of analyzing wing loads was investigated in the light of these findings.

The data for this work were recorded on a Lockheed C-130B airplane as it performed roller coasters between load factors of - 0.10 and 1.94 (extreme values attained) at equivalent air speeds between 143 and 338 knots at an altitude of approximately 10,000 feet.

The air loads were found to vary versus dynamic pressure and angle of attack with sufficient linearity to permit extrapolation to zero airspeed and to higher angles of attack and speeds, as done in the "slope-intercept" method of load analysis. This method has been applied to both straight wing, subsonic and supersonic, and swept wing airplanes with some success. No parameters, other than those noted, need be considered in computing total load; however, power effects should be evaluated before comparison of the loads with airload distributions or wind tunnel data for propellers off. Rate of change of angle of attack, pitching velocity, and flutter have a negligible effect on the final results for the C-130B airplane. Pitching acceleration was too small to be detected.

CHAPTER I

INTRODUCTION

The analysis of wing loads recorded in symmetrical flight maneuvers requires the examination of loads from several maneuvers to find the variation of load with acceleration, airplane weight, wing inertia, and speed. The loads are extrapolated to flight conditions at higher speeds and higher accelerations and compared to the strength of the airplane to determine whether the airplane may be safely flown to the extrapolated conditions. This procedure is necessary because actual flight loads are sometimes greater than loads calculated from wind tunnel data.

The flight conditions for these maneuvers must be described in terms of the aerodynamic conditions (airspeed, altitude, etc.), accelerations, airplane and fuel weight, and power. Also, the effects of these variables on the wing loads must be evaluated. This paper presents an investigation of the magnitude of the loads caused by these variables in order to improve the accuracy of the analysis of wing loads recorded in flight.

Howland and Buzzetti (Reference 1) describe a technique of analyzing wing loads recorded with the use of strain gages. The analysis presented here employs the same technique, which will hereafter be called the "slope-intercept" method. By use of this method the wing air loads are separated into air loads at zero load factor (zero-g or

weightless condition) and unit additional air loads (incremental air load per pound of nW--load factor times airplane gross weight). These are expressed as shear, bending moment and torsion due to loads outboard of the strain gage stations. Reference 2 describes the calibration of the strain gages for the measurement of flight loads.

Assumptions implicit in the slope-intercept method are:

1. The primary parameters for defining wing loads, nW and airspeed, have the following effects:

   a. Wing loads are linear with nW.

   b. Wing air loads at zero load factor may be extrapolated to zero air speed with no significant error.

2. The effects of the secondary parameters, such as power, pitching velocity, and pitching acceleration, are insignificant, or they are eliminated by averaging the increasing-g and decreasing-g loads in the push-pull maneuver.

Airframe manufacturers and government agencies have used the slope-intercept method of analysis for several years, apparently with success. The accessible technical papers that mention this method only state the first assumption; they do not present analyses of the method or justify the second assumption.

In using the slope-intercept method the writer and his associates have asked many questions concerning the validity of the assumptions: Can the air loads at zero load factor be extrapolated to zero air speed without significant errors? What effect does power have on the loads--are air loads on the propeller-plus-nacelle great enough

to invalidate the design assumption that all air loads are on the wing? Are transient effects large enough to affect the loads?

Some variations observed in the results obtained from the slope-intercept method have been attributed to the normal scatter of flight test data; however, no literature has been discovered that gives the extent to which the slope-intercept method itself may contribute toward these variations. Various papers on the measurement of flight loads are listed as References 3 through 6.

The purpose of this investigation is to show the effect of certain flight parameters on wing loads. These parameters are speed, power, angle of attack, rate of change of angle of attack, pitching velocity, pitching acceleration, and flutter; each parameter to be investigated separately. This analysis extends the approach found in the literature by giving a method of evaluating the effect of the parameters noted above and by showing an example of the effects of these parameters on wing loads recorded in symmetrical flight maneuvers.

The loads for this investigation are recorded with the use of strain gages. The test maneuver is the "roller coaster," a symmetrical flight maneuver with no abrupt control motions. Since the writer has access to data recorded on the Lockheed C-130B he will analyze the data obtained during one series of test maneuvers performed by this airplane. Flight test data on the C-130A and the C-130B are given in References 7, 8, and 9. Aerodynamic and weight data on the C-130B are given in References 10 and 11.

CHAPTER II

METHOD OF ANALYSIS

Purpose of Measuring Wing Loads

The purpose of measuring wing loads is to determine the difference between the actual and the theoretical spanwise air load distributions on the wing. The results of the measurements are compared to wind tunnel or calculated spanwise distributions, or they are extrapolated to the desired weight, speed, and load factor for comparison with wing strength or design loads.

Test Maneuver

In order to provide wing loads for analysis the test maneuver must cover a sufficient range of load factor and speed to permit the extrapolation of loads to the design maneuver points, the spanwise air loading at these points being the ones of primary interest. The airplane gross weight, center of gravity, fuel loading, and flight altitude should be maintained as near constant as possible to eliminate load variations due to changes in any of these parameters. The maneuvers should be performed smoothly to eliminate any transients or load distributions caused by abrupt motions. The maneuvers must be performed as quickly as possible to reduce speed changes during the maneuver. Within these requirements and limitations the most satisfactory maneuver is the "roller coaster."

The roller coaster is performed as a push-down to near zero g's (weightless condition) followed by a pull-up to the desired load factor and a recovery to unaccelerated flight. The desired load factor may be 2.0 for a bomber or transport airplane and 3.0 or more for a fighter or a trainer. The control motions should be smooth enough to reduce the effects of transients yet fast enough to minimize the speed change. A sample time history of a roller coaster is shown in Figure 1.

The maneuver is usually performed in four to ten seconds. Note that in Figure 1 neither the elevator motion nor the load factor is sinusoidal. The usual procedure is for the pilot to push the control column forward to cause the airplane to nose over. When the load factor is about 0.1 above the desired minimum the pilot pulls the control column back smoothly to stop the push-over and start the pull-up. Every maneuver will be a little different from every other because the control forces and the airplane response change with speed and because the pilot is human.

This single maneuver provides loads throughout a range of load factors at one speed and for constant airplane gross weight, center of gravity, fuel distribution, power, and altitude. A series of roller coasters throughout the speed range can be performed in a few minutes, keeping changes due to fuel consumption low.

The roller coaster maneuver may be used throughout the speed and load factor range of any airplane unless limited by stall, pitch-up, buffet, or by temperature differentials between parts of the structure to which gages of a single bridge are attached.

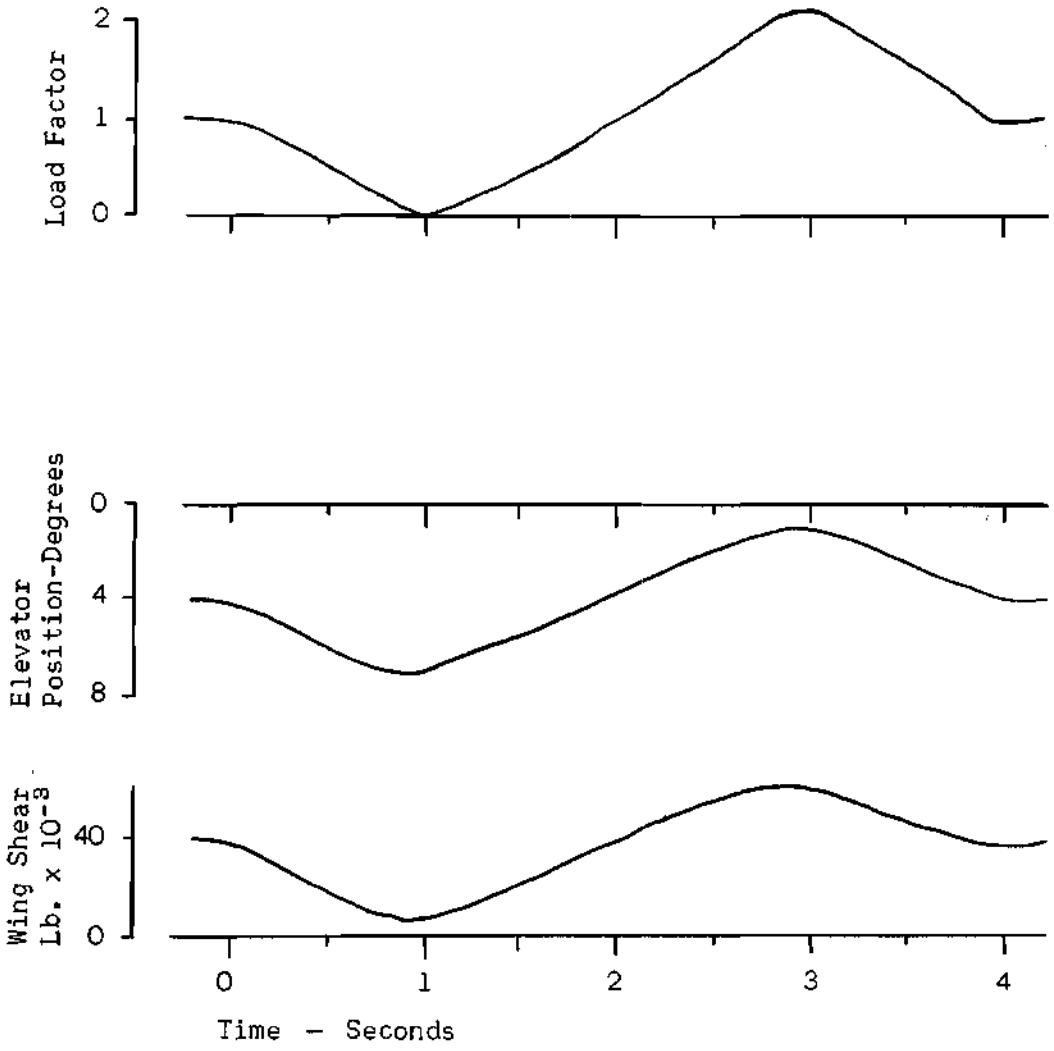

Figure 1. Time History of a Roller Coaster Maneuver

Methods of Measurement

Total wing loads are measured with strain gages attached to the structure at several spanwise locations. The gages are installed, combined electrically and calibrated to respond linearly to the shear, bending moment, and torsion at each gage location (wing station).

The strain gages are usually bonded to the web and caps of each major spanwise beam, as shown in Figure 2(a). The gages are sensitive to strain in the lengthwise direction. They are relatively insensitive to transverse strain. The gages on the caps are sensitive to axial loads in the beam caps. They are wired into a Wheatstone bridge, as shown schematically in Figure 2(b), to respond to the vertical bending on the beam. The gages on the web are wired to respond to shear. In a wing structure with two or more beams the outputs of shear bridges on two beams are added electrically to respond to wing shear, subtracted to respond to torsion. While this type of installation is common, it is not the only one. Gages are installed in the upper and lower skin, for example, to record torsion or bending. They may be attached to the outside of the wing as well as to the inside. Gages installed in a swept wing respond linearly to externally applied loads just as in a straight wing. The types of installations are limited by the types of wing structure, the ingenuity of the engineer, and the ratio of strain bridge output to the background noise of the electrical circuits. The most satisfactory installation is in a uniform structure that responds linearly to loads. This calls for shear resistant webs and for the avoidance of stress concentrations, as near fittings, cutouts, sharp

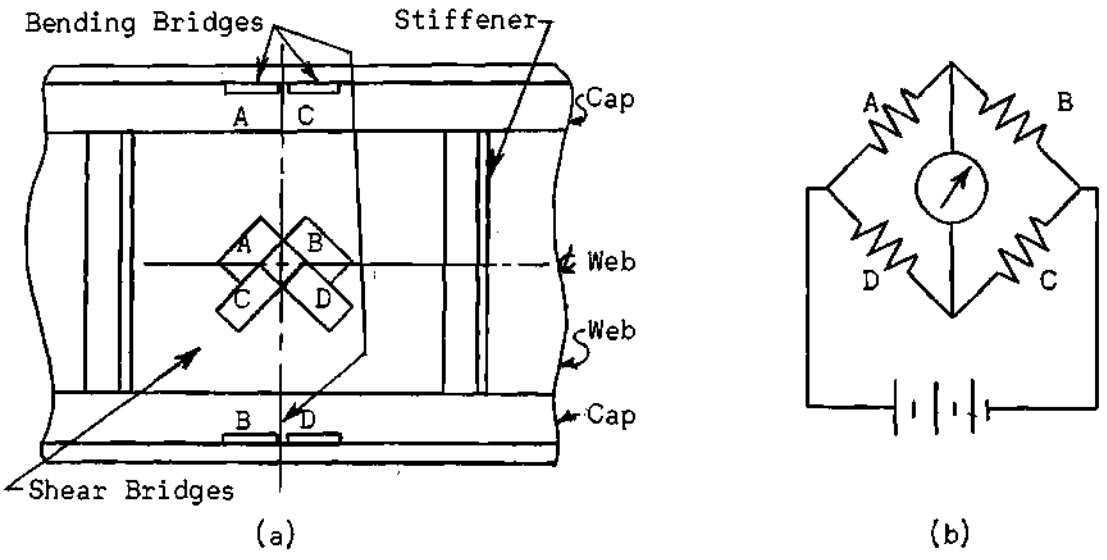

Figure 2. Strain Gage Installation

radii, etc. The strain gages on the Lockheed C-130B wing are installed at five spanwise stations, as shown in Figure 3.

Strain gage bridges respond to loads applied to the wing outboard of the gage station; hence the spanwise and chordwise centers of pressure of the entire surface may be obtained from the shear, bending moment, and torsion at a single gage station at the wing root. Gages are usually installed at additional spanwise stations to furnish data for determining the shape of the spanwise loading distribution. One measure of the accuracy is the agreement of the bending moment data points to a spanwise integration of a curve passing through or near the shear points. The nearer the shear curve and its integral approach the data points, the better the data.

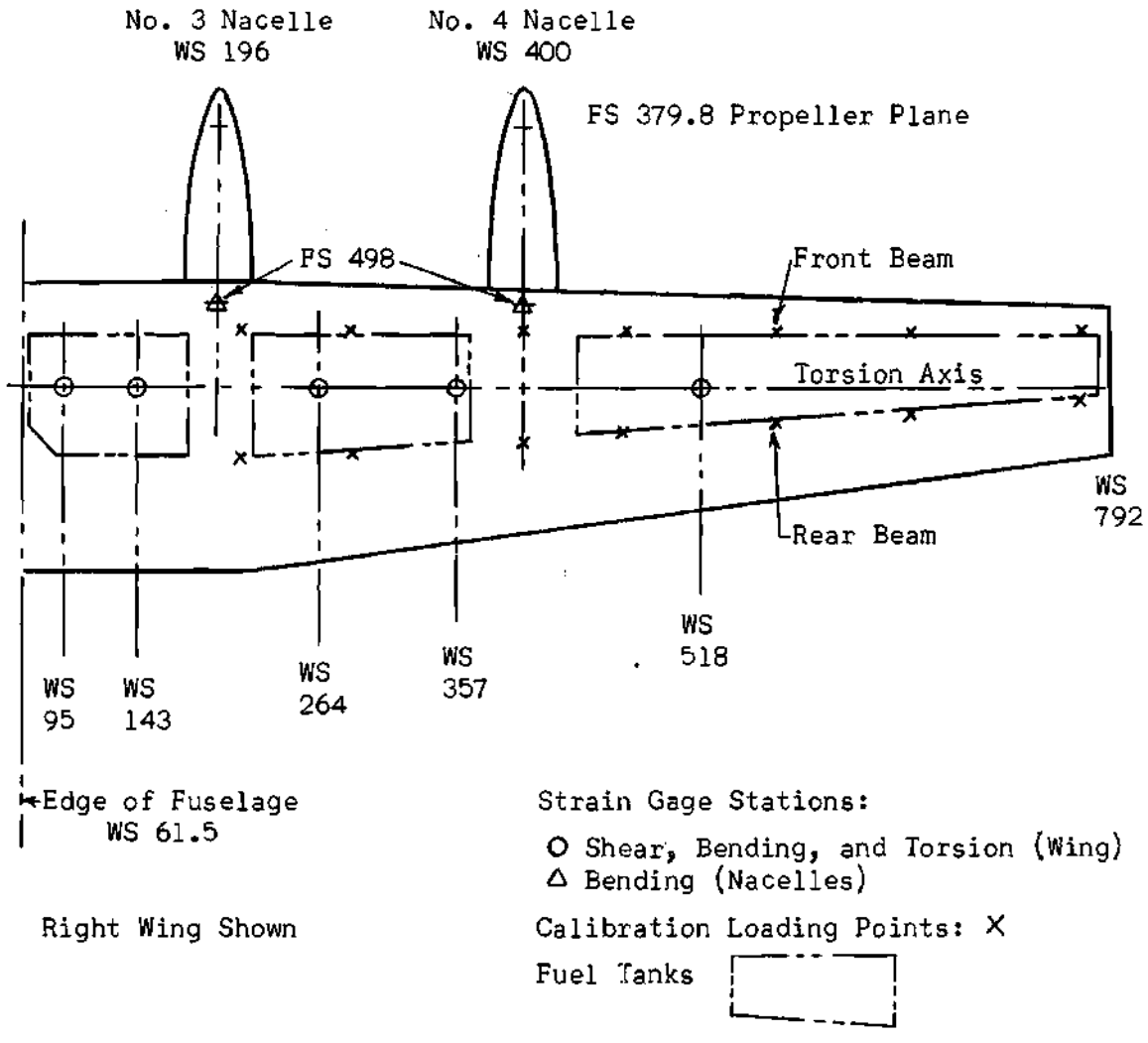

Figure 3. C-130B Wing Geometry and Strain Gage Stations

The number of gage stations is dictated by the need for data. A large number of gage stations are required on a new design being tested for the first time or on an existing wing where the addition of external stores, nacelles, etc., may cause local changes in the air load distribution. A small number of stations may furnish sufficient

data on a modification to an existing design where the aerodynamic shape is unchanged.

The bridges are calibrated by the application of point loads, applied singly, at several spanwise and chordwise locations and by the reading and plotting of the bridge outputs. The loading points are usually along two or more major beams in the wing at intersections with relatively heavy ribs. Usually pads are used to distribute a load along a beam. Also, auxiliary jigs are used to permit loads centered between the beams to be applied to the beams. These methods allow higher calibrating loads without structural damage than would be possible at weaker or single points in the structure. Additional loads may be applied to propeller shafts, engine mounts, and flap surfaces as desired. Typical loading points are shown in Figure 3.

The calibrating loads are applied in increments, 20 per cent for example, up to the maximum with the load stabilized and readings taken of all bridges at each increment. After the 100 per cent reading is taken the load is increased about 5 per cent, then reduced to 100 per cent and a "decreasing load" reading taken. The load is decreased to zero in similar decrements with readings at stabilized loads on the way down. This procedure assures the same number of readings for decreasing load as for increasing load. No readings are taken at zero load as residual stresses frequently cause erratic readings at this point.

The response of each bridge for each loading point is determined by plotting the electrical output versus the load and taking the least-squares slope. This establishes the slope of the response versus load,

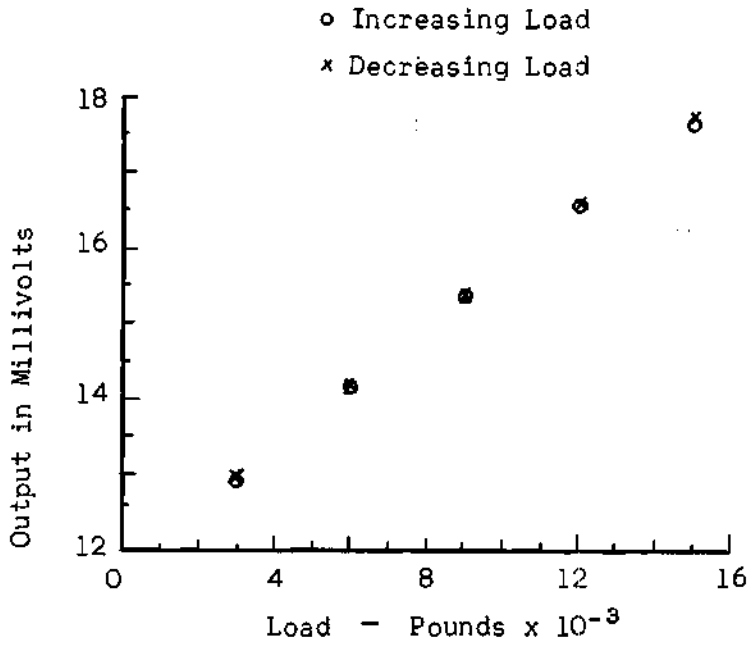

Figure 4. Bridge Output Versus Applied Load

but does not establish the bridge output for zero load. A sample plot is shown in Figure 4, above.

The sensitivity of strain bridges to the spanwise and chordwise position of the load is determined by plotting the electrical output, in millivolts per volt (or current applied to the circuit) per thousand pounds of load, versus wing station and fuselage station, as shown in Figure 5. This figure shows the response of shear bridges and moment bridges versus wing station and of a shear bridge versus fuselage station. These plots show that each bridge may be affected by both spanwise and chordwise variations in the center of pressure. The unwanted effects may be eliminated by combining the outputs of two or more bridges. In the case of the shear bridges in Figure 5(a) these effects may be eliminated by subtracting part of the output of a bending bridge and

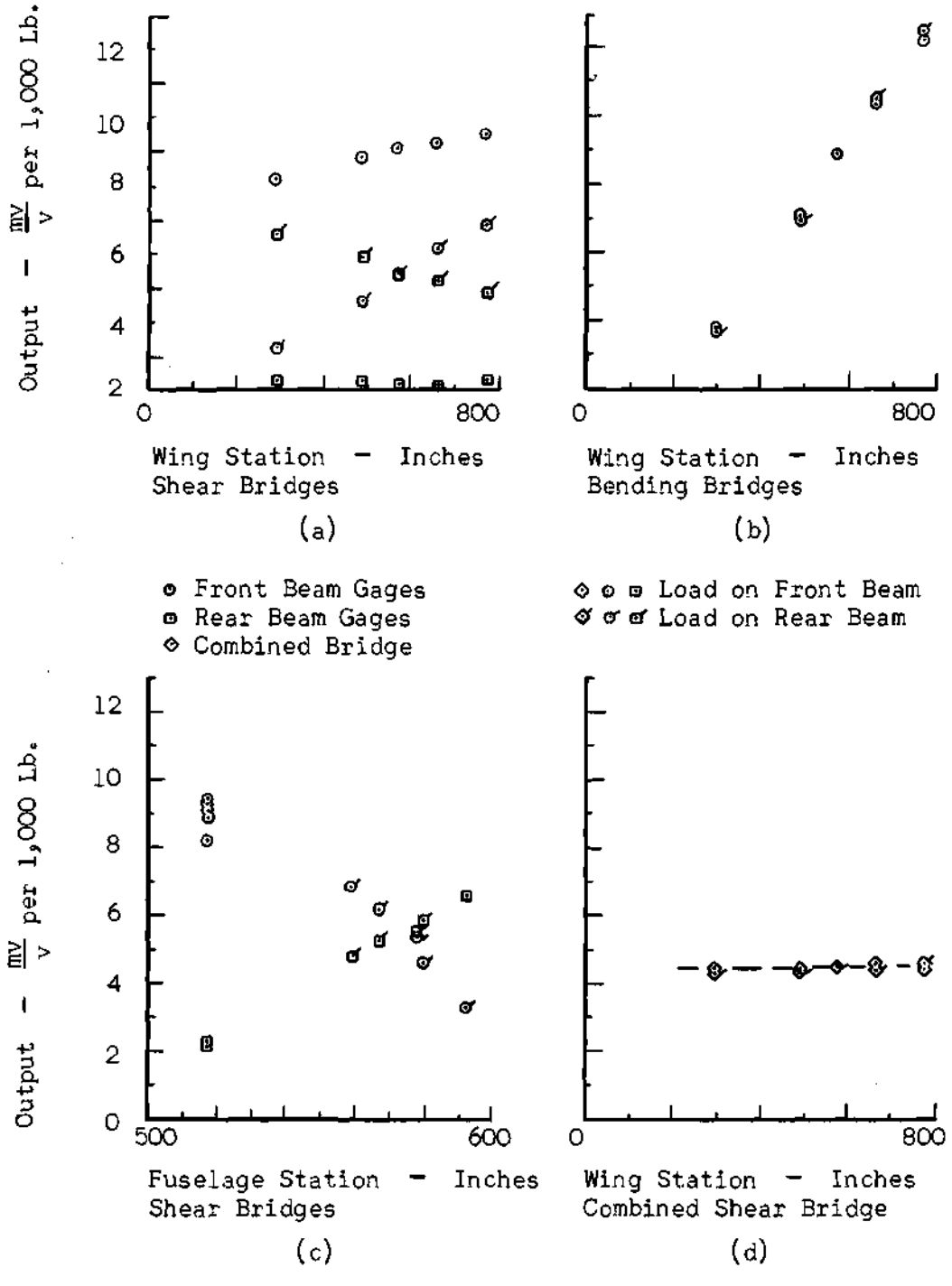

Figure 5. Influence Coefficient Plots

adding the outputs from shear bridges on both the front and rear beams. The output of the final combination is shown in Figure 5(d).

For a small number of bridges these corrections, or attenuations, can be made easily with hand calculations. For the Lockheed C-130B wing, with five spanwise stations, with gages on front and rear beams, with sufficient gages to allow combinations of bridges for removing unwanted effects, and with a full set of spare gages, hand calculations are impractical and machine methods must be used. The C-130B calibration was made using the method of Reference 2. The procedures were the same as those described for the C-130A calibration in Reference 12. No calibration report was written for the C-130B.

The nacelle strain gage installation consists of gages bonded to members of the engine mount truss. These gages respond to axial loads in the members to which they are attached. Calibration consists of applying vertical loads to a structural ring in the nacelle and calculating the bridge response by hand (see Reference 2).

The strain bridge outputs are recorded by use of recording oscillographs.

Accuracy of the Data

The overall accuracy of the data depends on the accuracy of each part of the system--the strain bridges, the recording system, and the data reduction.

The strain bridges are the only part of the system in which the probable error is evaluated mathematically. It is based on the deviation of the slope of the electrical response of each calibrating load

from the mean, as described in Reference 2. The following tabulation of probable error for the wing strain bridges of the Lockheed C-130B test airplane are taken from unpublished calibration data.

Probable Error--Per Cent of Maximum Calibrating Load

Load Wing Station	Shear	Moment	Torsion
95	0.4	0.8	2.1
143	0.3	0.8	1.6
264	0.4	0.6	0.3
357	0.8	0.8	5.9
518	0.8	1.0	3.3
Average	0.5	0.6	2.6

An examination of the averages shows that shear and bending moment are more accurate than torsion, verifying the writer's experience. The torsion at WS 357 would have less error if the nacelle load effect were ignored.

The recording system consists of the oscillograph, the balance and junction boxes, the power supply, and the wiring connecting these parts to each other and to the strain gages. The main sources of error within this system may be errors in the calibration resistors, voltage fluctuations, resistance errors due to the long wires to the strain gages, non-linearity and poor damping of the galvanometers, and galvanometer vibrations caused by the oscillograph shaking. The accuracy of the recording system has not been established in the precise manner used for strain gages. The Instrumentation Department of Lockheed's

Engineering Flight Test Division considers the overall accuracy of the recording system to be two per cent.

The data reduction consists of establishing the sensitivity of the trace on the paper record, reading the deflection from a convenient reference, and converting the deflections to loads. The sensitivity is determined by the height of the calibrate step. This step is caused by the addition of a known resistance into the strain bridge circuit and is equal to the trace deflection caused by a predetermined load. The load per inch of the trace is this predetermined load divided by the step height in inches.

The reading accuracy for this procedure has been estimated as ± 0.01 inch for the step height and ± 0.04 inch for the trace position by the Data Reduction Group of the Engineering Flight Test Division. The step height can be read more accurately because the lines involved are flat and smooth. The trace position is more difficult to read because of the continual oscillations at 40 to 70 cycles per second due to the propeller passage frequency and the vibration of miscellaneous masses in the airplane and because of the steepness of the trace at various times. Another source of error is the variation of the step height throughout the flight, usually 0.02 inch or less, from the value used for calculating the trace sensitivities.

The average step height is one inch, so the relative accuracies of reading and step height variation are one and two per cent, respectively. The average double amplitude of trace deflection in a roller coaster is two inches, giving two per cent accuracy in the trace reading. Figure 6 represents a typical oscillograph record trace.

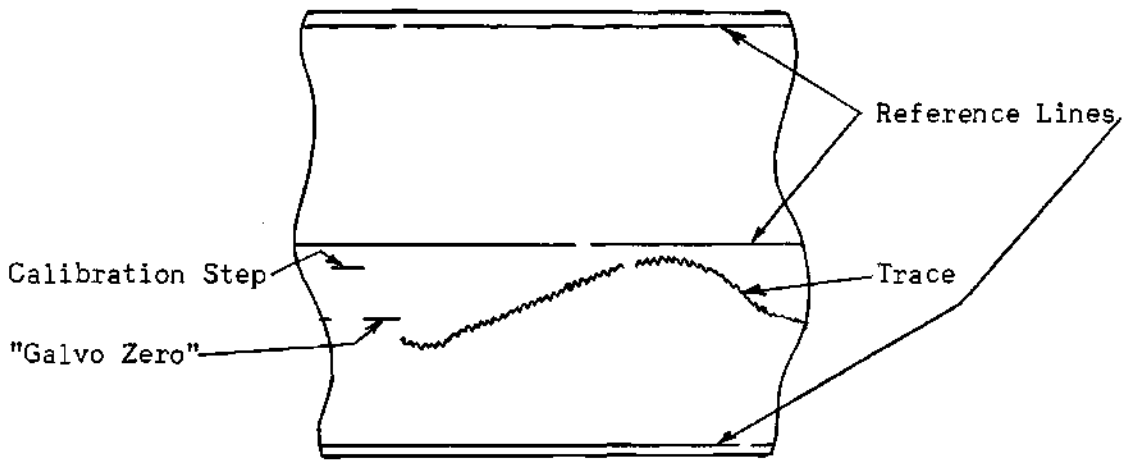

Figure 6. Oscillograph Record

A rough approximation of the total slope error is calculated as the square root of the sum of the squares of the errors of the parts--strain bridges, recording system, reading errors, and step height variations.

$$E(\%) = \sqrt{(1)^2 + (2)^2 + (1)^2 + (2)^2 + (2)^2}$$

$$= 4\ \%\ .$$

This value is an approximation for use in evaluating certain parameters discussed later in this paper. It is not a statistical study of the accuracy of flight test data.

Data Recorded in Flight

The data recorded in flight are:

1. Flight conditions: airspeed, altitude, free air temperature, and load factor at the airplane center of gravity.

2. Engine data: (for each engine) torque, turbine rpm, turbine inlet temperature, and total fuel consumed.

3. Wing loads: vertical shear, vertical bending moment, and torsion about an arbitrary axis for loads outboard of a wing station where the strain gages are located. Strain gages are located at five stations on the right wing. More strain gage stations on the wing would improve the spanwise picture of the loads as well as reduce the reliance that must be placed on the accuracy and linearity of each bridge, particularly near the wing root.

4. Nacelle loads: vertical bending moment at the root of the nacelle for loads forward of the strain gages. Strain gages are installed on both nacelles attached to the right wing.

5. Empennage loads, control surface positions and hinge moments, accelerations at numerous locations throughout the airplane, angles of attack and sideslip. These are recorded in the evaluation of other maneuvers and for back-up information to aid in the explanation of unexpected phenomena.

The flight conditions are measured with standard type equipment. The aneroid instruments are connected to ports on the tip of a boom as far away from disturbing airflow as possible. On the C-130B the boom is located on the right wingtip with the pressure ports about one chord length ahead of the leading edge of the wing. The accelerometer is located on the front beam of the wing at the airplane centerline. This is within five inches, fore and aft, of the airplane center of gravity. The engine data are recorded by standard tachometers, torque meters,

and by integrating flow meters. The fuel aboard is the measured amount at engine start less the fuel consumed.

Method of Analysis

The purpose of analyzing flight test loads is to express them in a form suitable for further calculations. These calculations include comparison to theoretical loads and extrapolation to higher speeds and load factors. The form of the data must account for the effects of all significant variables.

The forms adopted for this task are the "unit additional air load" and the "zero-g air load" shear, bending moment, and torsion. The unit additional air load is the additional air load per pound of airplane nW. The zero-g air load, selfexplanatory, is the basic air load plus enough positive additional air load to equal the down air load on the fuselage and the tail, balancing the total vertical air load to zero, as shown in Figure 7. The additional air load part of the zero-g air load equals the magnitude of the fuselage and tail air load.

The total air load is expressed as:

$$L = L_{n=o} + \frac{L}{nW} \cdot nW \qquad (1)$$

where

$L_{n=o}$ = Zero-g air load

$\frac{L}{nW}$ = Unit additional air load .

While these air loads are not directly comparable with the customary spanwise lift distributions, the spanwise distributions may be integrated

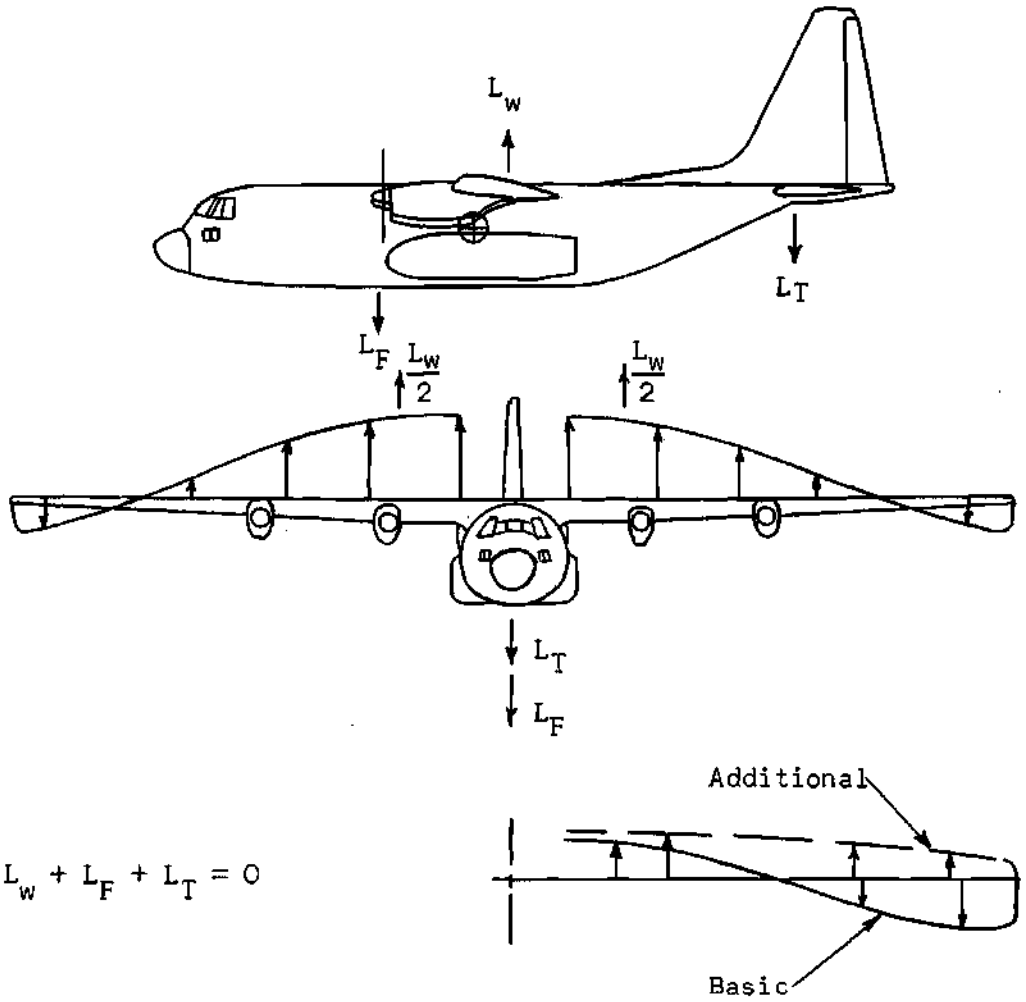

Figure 7. Air Loads at Zero-g

and converted to the same dimensions as the flight loads for comparison.

Another problem affecting the method of analysis is the poor repeatability of a ground static reading corrected for inertia. This zero shift has been attributed to residual stresses caused by temperature differences between various parts of the structure, fabrication methods, slippage between parts, etc.

The solution is to plot recorded loads versus load factor, remembering that the loads are read from an arbitrary reference line. This is done for each data trace for each roller coaster, and the loads are extrapolated to zero-g where the inertia becomes zero and only air load remains. A sample plot of load versus load factor is shown in Figure 8. These zero-g points are plotted versus dynamic pressure and extrapolated to zero dynamic pressure where the air load becomes zero. Since air and inertia loads are the only forces involved, this intercept at zero-g and zero dynamic pressure defines the zero load reading on the arbitrary scale. All readings are corrected to refer to this point, as shown in Figure 9.

The load per $g(\frac{\Delta L}{\Delta n})$ is converted into unit additional air load $(\frac{\Delta L}{\Delta n W})$ by the removal of the inertia from the total load per g and by division by the gross weight.

$$\frac{\Delta L}{\Delta n} = \frac{\Delta L}{\Delta n W} + L_i \ ,$$

or

$$\frac{\Delta L}{\Delta n W} = \left(\frac{\Delta L}{\Delta n} - L_i\right) \frac{1}{W} \tag{2}$$

$$L_i = L_{wi} + L_{if} + L_{of} \tag{3}$$

where subscript i = unit inertia of wing plus fuel,

wi = unit inertia of wing alone,

if = unit inertia of fuel in inboard tank, and

of = unit inertia of fuel in outboard tank.

The static balance of the airplane is expressed in coefficient form based on the following assumptions:

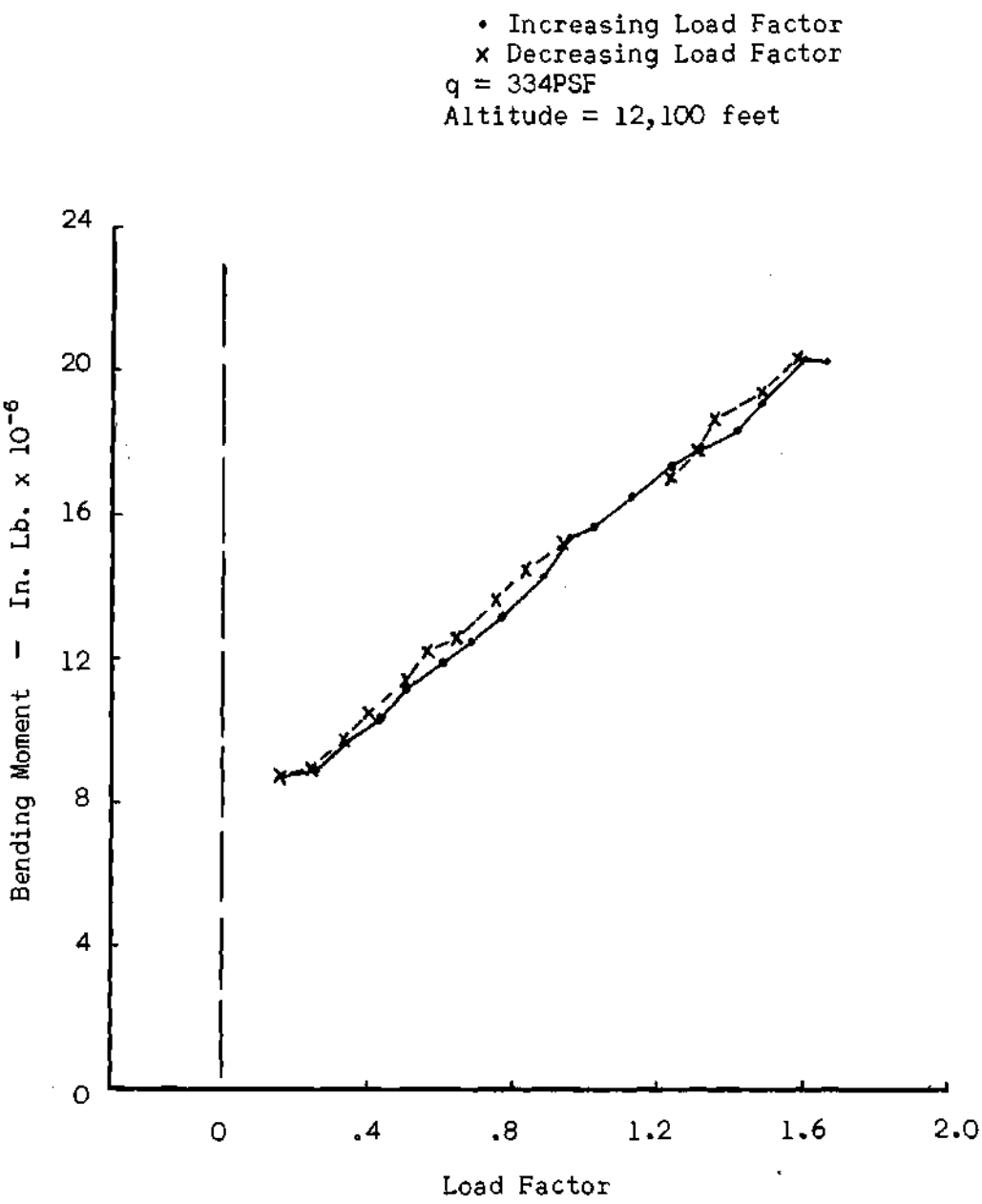

Figure 8. Bending Moment Versus Load Factor (Data Points)

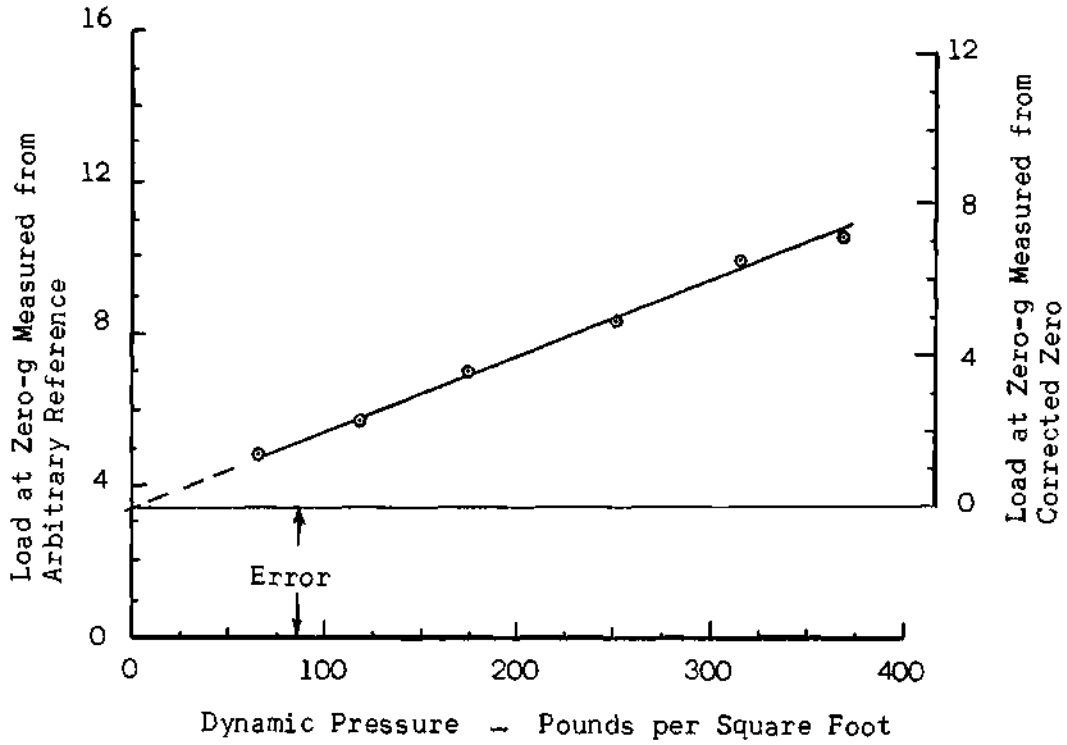

Figure 9. Load at Zero-g Versus Dynamic Pressure

1. All coefficients are based on the wing area, S.

2. Distances forward of the aerodynamic center are positive.

3. Moment is taken about the aerodynamic center of the airplane minus tail.

4. The center of lift on the horizontal tail is close enough to the quarter-chord point of the mean aerodynamic chord of the horizontal tail, $(\bar{c}/4)_t$, so that no significant error is introduced by the use of this point.

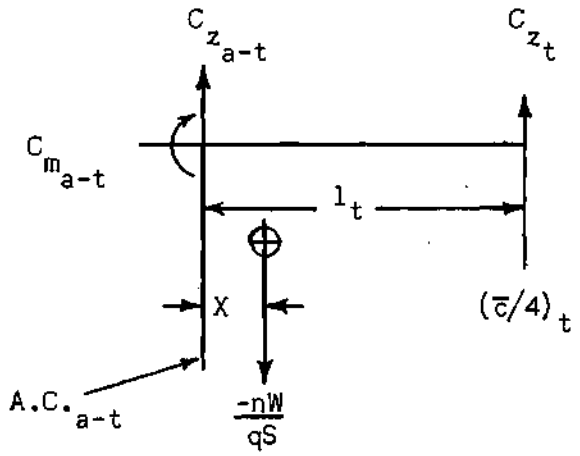

$$\Sigma C_z = 0, \quad C_{z_{z-t}} + C_{z_t} + \frac{-nW}{qS} = 0 \tag{4}$$

$$\Sigma C_{m_{AC}} = 0, \quad C_{m_{a-t}} + C_{z_t} \cdot \frac{l_t}{\bar{c}_w} - \frac{nW}{qS} \cdot X = 0 \tag{5}$$

$$C_{z_t} = \frac{1}{l_t}\left(\frac{nW}{qS} \cdot X - C_{m_{a-t}} \cdot \bar{c}_w\right) \tag{6}$$

where X is the distance from the airplane center of gravity to the aerodynamic center of the airplane minus tail.

Combining $$C_{z_{a-t}} - \frac{nW}{qS}\left(1 - \frac{X}{l_t}\right) - C_{m_{a-t}} \cdot \frac{\bar{c}_w}{l_t} = 0 . \tag{7}$$

At $n = 0$ this becomes

$$C_{z_{a-t}}\Big)_{n=o} - C_{m_{a-t}}\Big)_{n=o} \cdot \frac{\bar{c}_w}{l_t} = 0 . \tag{8}$$

The additional air load coefficients are

$$C_{z_{a-t}}\Big)_{ad} - \frac{nW}{qS}\left(1 - \frac{X}{l_t}\right) = 0 . \tag{9}$$

Equation (9) shows that the additional air load varies directly with the distance from the center of gravity to the aerodynamic center of the airplane minus tail. With this equation and the total additional air load at the center of gravity position one can obtain the corresponding air load at any other center of gravity. The air load and pitching moment coefficients on the airplane minus tail may be divided as follows:

$$C_{z_{a-t}} = C_{z_w} + C_{z_n} + C_{z_p} + C_{z_{ss}} + C_{z_f} \tag{10}$$

$$C_{m_{a-t}} = C_{m_w} + C_{m_n} + C_{m_p} + C_{m_{ss}} + C_{m_f} \tag{11}$$

where the subscripts signify:

w = Wing (less effect of slipstream),

n = Nacelle,

p = Propeller,

ss = Slipstream (effect on the wing), and

f = Fuselage .

The measured wing airloads and moments are the sums of the first four terms on the right-hand side of Equations (10) and (11) that act on the wing outboard of the strain gage station at which they are measured. The nacelle bending moments include the sum of the effects of the second and third terms on the right-hand side. Fuselage loads are not measured directly.

Use of this method requires several roller coasters throughout a large enough speed range to establish a curve of zero-g air load

versus dynamic pressure and a low enough minimum speed to permit extrapolation of the zero-g air load to zero airspeed without the likelihood of significant error. The definitions of satisfactory speed ranges, minimum speed and of acceptable error are, at present, matters of experience and judgment. They are not within the scope of this investigation.

Analysis of the Effect of Various Parameters

Basis for the Selection of Parameters.--Each parameter that varies during one series of roller coasters is examined to determine the nature of its effect on wing air loads and the desirability of further examination.

Gross Weight.--The total lift on the airplane is a direct function of the gross weight. This effect is discussed under Angle of Attack.

The change in gross weight from one maneuver to another is accounted for in the method of analysis by using the exact weight during each maneuver for the calculations involving that maneuver. The weight change during a maneuver at the hypothetical fuel consumption of 10,000 pounds per hour in a roller coaster of six seconds duration is 17 pounds, hence insignificant for any existing airplane.

If the weight change during a series of roller coasters appears sufficiently large, in the engineer's judgment, to affect the lift distribution the effect can be proved by a set of roller coasters starting at a much higher (or lower) gross weight than the first set.

Center of Gravity.--During one set of roller coasters the center of gravity will shift if the center of gravity of the fuel consumed is different from that of the gross weight of the airplane. The effect of this shift on the wing load can be evaluated from the loads recorded in a second set of roller coasters, the center of gravity for the second set at either extreme forward or extreme aft position, whichever is farther from that of the first set.

Since one set of roller coasters is insufficient to evaluate the effect of center of gravity position, this effect is not investigated further.

Altitude.--Although the altitude should be constant for all roller coasters of one series, it does vary from one maneuver to the next, particularly at high speeds which can be attained only by diving. The writer's experience has been that the variation is usually less than ± 500 feet. One exception should be noted in the test data of Table 2.

The effect of this altitude change may be evaluated by comparing loads from roller coasters performed at altitudes different by several thousand feet. As this requires two sets of roller coasters it is beyond the scope of this study.

Angle of Attack.--Wing and total airplane lift vary with angle of attack, the variation being approximately linear except when separation occurs. This linear variation appears in wing shear, bending moment, and torsion at various span stations as a straight line slope of these items versus angle of attack.

Actually angle of attack is not a satisfactory parameter because of insufficient accuracy of measurement at high speeds and inconvenience in calculations. The angle of attack is measured by an electrical device sensitive to the angular position of a shaft on which a vane is mounted. The whole assembly is mounted approximately one chord length ahead of the right wing tip. The accuracy, estimated by the Instrumentation Department of Engineering Flight Test, is ± 0.5 degree. It is easy to see that this wing tip angle of attack may not be sufficiently accurate for establishing a lift curve slope from data taken at high speeds. It is sufficient to establish the existence of wing twist versus speed where the angular variations are in the order of degrees. The load factor measurements are estimated by the same organization to be within 0.1 g. Over a range of two g this is ten per cent of the total range; however the fairing of the data points may be expected to reduce the probable error to a much lower value.

Wing loads are linear with angle of attack, as is weight times load factor (nW). Since they are linear with respect to the same variable, they are linear with respect to each other. Use of load factor times weight instead of angle of attack shortens the calculations and improves the accuracy.

The linearity is investigated by determining the variation of the measured loads versus load factor.

Speed.--The effect of speed appears in the basic air load as a linear variation of the load with dynamic pressure so long as the terms of Equation (8) are constant.

If the terms of Equation (9) are linear versus angle of attack the unit additional air load is constant versus speed.

Pitch Angle, Longitudinal Acceleration, and Change in Velocity During a Maneuver.--These parameters are not investigated as neither pitch angle nor longitudinal acceleration are available, and lag in the airspeed system prevented instrument response to the change in velocity.

Elevator Position and Motion.--Before the effect of elevator position and motion on the wing loads is evaluated the effect of these parameters on the tail load must be evaluated. Since no data are available for this analysis no further investigation is made.

Rate of Change of Angle of Attack.--Any change in wing air load due to rate of change of angle of attack ($\dot{\alpha} = \frac{dq}{dt}$) appears on the load versus load factor plots as a separation of the "$+\dot{\alpha}$" points from the "$-\dot{\alpha}$" points, causing a line connecting time-consecutive points to form a loop. Interpolation between these points to obtain the load at zero $\dot{\alpha}$ will eliminate this parameter from the data.

Pitching Velocity.--The pitching velocity affects the elevator deflection required to produce a given tail load but has no effect on the tail load required to balance the airplane. Consequently it has no effect on the wing load.

The gyroscopic loads from the engine and propeller due to pitching velocity act in the horizontal plane only.

Pitching Acceleration.--Pitching acceleration is caused by the amount of horizontal tail load different from that required to balance the

airplane and satisfy Equation (5). This incremental tail load causes a change in the load factor for a given airplane-minus-tail air load indicated by Equation (4). This unbalance appears on the load versus load factor plots as a low wing load for a given load factor in negative pitching acceleration (positive incremental tail load) and a high wing load for positive pitching acceleration. These would normally occur in the push-over and pull-out parts of the roller coaster, respectively. The deviation from normal is proportional to the pitching acceleration.

Also, wing and nacelle loads may be affected by the pitching acceleration of large mass items some distance from the center of gravity of the airplane.

Proper evaluation of the effect of pitching acceleration requires sufficient accelerometers to measure this acceleration. Since the C-130B was not instrumented for this, any evaluation must be on the basis of estimated accelerations.

Flutter.--Flutter will appear as a load oscillation superimposed on the load due to load factor. If the flutter oscillation is at the same frequency as the roller coaster the loads due to these two causes are inseparable and this method of analyzing wing loads is impractical. The flutter load appears as a large loop in the load versus load factor plot. The loops vary from one roller coaster to the next as the frequency of each roller coaster is unique due to human inability to perform each maneuver in exactly the same time.

If the flutter oscillations are at frequencies higher than that of the roller coaster the flutter loads will appear on the load versus

load factor plots as deviations from a straight line such as those shown in exaggerated form in Figure 10. This figure shows amplitude versus sin ωt for two superimposed oscillations. The larger amplitude oscillation at the lower frequency represents the variation of load versus load factor. The smaller amplitude oscillation, at higher frequencies, represents the flutter. The total amplitude may be expressed as

$$\text{Amplitude} = A(\sin \omega t + 0.5 \frac{f_2}{f_1} \sin \omega t)$$

where A = amplitude due to the low frequency oscillation

$$\frac{f_2}{f_1} = 1.5, \quad 2.0, \quad 2.5, \quad 3.0, \quad \text{and } 4.0.$$

As shown, the addition of the flutter load causes a variation of the load from a straight line, but does not change the slope. Hence, higher frequency oscillations have no effect on the slope of the net load versus load factor. The higher the superimposed frequency, the easier is the determination of the average slope.

Power.--The effects of power on the wing loads appears as propeller loads applied through the nacelles and slipstream loads applied directly to the wing. The best method for determining these effects is to perform one set of roller coasters with power for level flight and another set with all propellers on the instrumented wing feathered, the difference between the two sets of loads being the effect of power.

This procedure cannot be used on the C-130B as no roller coasters were performed with propellers feathered. Also, the propeller loads are recorded by a bending bridge in each nacelle, hence cannot be obtained separate from the nacelle loads.

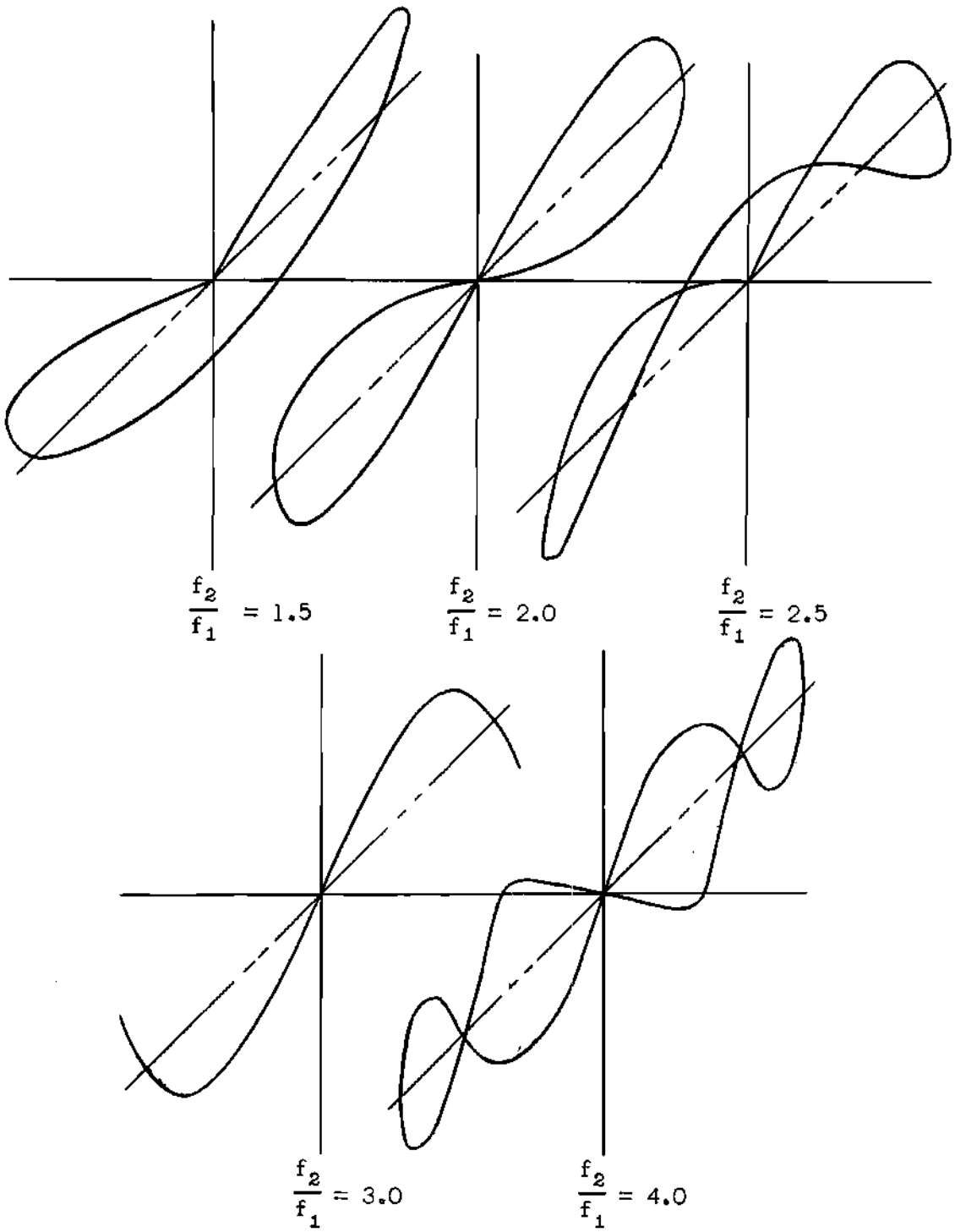

Figure 10. Higher Frequencies Superimposed on an Oscillation

The propeller and nacelle loads can be separated by calculating the propeller loads by the method described by Rumph, White and Grumman in Reference 13, and then subtracted from the total nacelle moment to give loads from the nacelle alone.

The equation for the propeller normal force in Reference 13 is:

$$C_z = R_1 \frac{D^2}{S} \alpha_p \tag{12}$$

where

$$\alpha_p = 1.32(\alpha_{FRL} + 0.7^\circ) \qquad \text{(degrees)} \tag{13}$$

R_1 = $M_1 C_T + M_2 B$

M_1 = function of J and thrust distribution along r (radius of propeller)

M_2 = function of J and blade shape

B = number of blades per propeller .

The equation for the propeller pitching moment coefficient is:

$$C_M = R_4 \frac{D^4}{S\bar{c}b} \cdot \frac{\dot{\theta}b}{2V_T(fps)}$$

$$= R_4 \frac{D^4\dot{\theta}}{2S\bar{c}\ V_T(fps)}$$

where

$$R_4 = N_1 C_P - N_2 B .$$

N_1 and N_2 are functions of thrust distribution, blade shape and J.

In the calculations of pitching moment due to pitching velocity in Reference 13 the pitching velocity and rate of change of angle of

attack appear to be considered equal. This is the only possible assumption as the corrections for the wind tunnel tests used are not available.

CHAPTER III

DISCUSSION OF RESULTS

Angle of Attack.--An examination of the typical load versus load factor plots, Figures 11 through 18, shows that the load varies nearly linearly with load factor, hence with angle of attack, within the scatter band. Thus one of the assumptions of the slope-intercept method of analysis is verified.

The plots of unit additional air load versus dynamic pressure, Figures 19, 20, and 21, show that the lift curve slope increases with speed.

If the variation of load is nonlinear with respect to load factor the slope-intercept method may still be used. In this case the curvature of the load versus load factor must be determined first. The inertia, which is linear versus load factor, is subtracted from the net load, leaving the same curvature as before, but a different initial slope. Details of handling the data may be different, but the validity of the method is not affected.

Speed.--The effect of speed appears principally in the zero-g air loads, Figures 22, 23, and 24. The loads increase linearly with dynamic pressure up to approximately 200 psf (V_e = 242 knots, M = 0.44) where the slope of the bending moment curve begins to fall off. The shear is linear versus dynamic pressure up to approximately 300 psf (V_e = 297 knots, M = 0.54). These changes show that flexibility can have

noticeable effects even on straight wings. The slope of the torsion curve, Figure 24, is nearly constant versus speed, indicating that it is caused mostly by C_{m_o}. The linearity of these loads at low speeds shows they may be extrapolated to zero airspeed without significant errors.

Since the fuselage angle of attack at zero-g does not vary with Mach number (stated in Reference 10) the variation of the wing tip angle of attack at zero-g with dynamic pressure, Figure 25, is a good indicator of the magnitude of wing twist with speed. Figure 25 verifies the wing twist suggested by the variation of the wing loads at zero-g with speed.

The static aeroelastic effect noted above may become significant in determining the variation of the zero-g air load versus dynamic pressure at low speeds for highly flexible wings, particularly at high altitudes where the minimum practical speed for a roller coaster may be as high as 0.6 Mach. In such cases it is desirable to have a curve of zero-g air load versus dynamic pressure calculated for a flexible wing and based on wind tunnel data. This curve can serve as an aid in extrapolating the test data to zero airspeed.

Rate of Change of Angle of Attack.--While the rate of change of angle of attack $(\dot{\alpha})$ is not directly available, average values are developed from unpublished readings of time and angle of attack and presented in Table 1. This table shows the values of $\dot{\alpha}$ to be lowest at high speed and greatest at low speed. It also shows the difference in $\dot{\alpha}$ between the increasing-g and the decreasing-g parts of the pull-out phase is greater than between corresponding parts of the push-down phase of the

roller coaster. In plain language, the recovery from the pull-out is more abrupt than the recovery from the push-down.

Examination of the plots of shear and bending moment versus load factor, Figures 11 through 14, shows that no spread exists between the increasing-g and decreasing-g points; therefore these loads are not affected by $\dot{\alpha}$. The pull-out portion of the wing torsion, Figures 15 and 16, shows a spread of 200,000 inch pounds at the lowest speed where both $\dot{\alpha}$ and the spread are maximum. Since neither shear nor moment is affected it appears likely that the torsional spread is caused by changes within the boundary layer.

The spread between the decreasing-g and the increasing-g points in the push-down is a maximum in Figure 18 for nacelle bending moment (30,000 inch pounds) and in Figures 15 and 16 for wing torsion (250,000 inch pounds). Since the spread in the wing torsion values is eight times the spread in the nacelle bending moment and does not always occur at the same time it appears that the nacelle plus propeller load has little effect on the wing torsion. The cause of this spread in the push-down is unexplained.

Pitching Acceleration.--The lack of spread between the increasing-g and the decreasing-g nacelle bending moments in the pull-out part of the roller coasters indicates that the pitching acceleration has no effect.

Flutter.--Flutter loads appear as small amplitude, relatively high frequency oscillations superimposed on the low frequency oscillations of the roller coasters. The fairing of the data removes any effect of the flutter loads from the zero-g and the unit additional air loads.

Power:--The significant propeller load calculated by the method of Reference 13 is the vertical load due to angle of attack, as shown in Table 2. This table also shows that the principal variables in this load are speed, as it affects J and q, the number of propeller blades, and the angle of attack. Of lesser importance is the shape of the blade, noted by I, II, and III in Reference 13. The shapes represented by these numbers are not given. The effect of thrust distribution along the blade was considered and found to be negligible for this airplane. The effect of C_T is small on this propeller. It would be larger on a three- or two-bladed propeller, since the effect varies inversely with the number of blades.

The contribution of the pitching moment due to $\dot{\alpha}$ is less than one per cent of the calculated load, as shown in Table 2. Since this is below the accuracy of the test data, this item is considered negligible and is omitted from future calculations.

The test values of nacelle bending moment for zero-g air load, presented in Figure 26, were extrapolated to zero airspeed, approximating the variation versus dynamic pressure of the loads calculated by the method of Reference 13 and shown on the same figure. The points at dynamic pressures of 158 and 226 pounts per square foot appear inconsistent with the remaining runs and are omitted as questionable data. The test loads increase positively with dynamic pressure where the calculated loads due to the propeller are negative. This shows that the air load on the nacelle is positive and is larger than the load due to the propeller.

The test values of unit additional air load on the nacelle, in Figure 27, are three to four times the calculated propeller load, indicating a large up air load on the nacelle.

The loads on the wing from the propeller-plus-nacelle loads have been calculated and the corrected loads added to the zero-g air load plots, Figures 22 through 24, and to the unit additional air load plots, Figures 19 through 21.

These figures show that the propeller-plus-nacelle loads are not over ten per cent of the zero-g air load shear on the wing. The moment is 500,000 inch pounds at high speeds, about four per cent of the total variation of the moment in the roller coasters. These loads have no significant effect on the shape of the curve or the extrapolated value at zero airspeed. The propeller-plus-nacelle loads may be ignored except when test loads are compared to wind tunnel propeller-off values of the zero-g air load.

The test values of the unit additional air loads on the wing corrected for propeller-plus-nacelle loads form smooth curves versus dynamic pressure with little scatter. Correction for these loads reduces the wing loads significantly, particularly the unit additional air load shear. This correction shifts the center of pressure of the unit additional air load outboard and aft, the aft shift being larger, as shown in Figure 28.

Test data should be corrected for propeller-plus-nacelle loads before being compared with loads based on power-off wind tunnel data; however these data need not be corrected for comparison of test and analytical total wing loads.

CHAPTER IV

CONCLUSIONS AND RECOMMENDATIONS

This investigation shows that:

1. The zero-g air load is sufficiently linear with dynamic pressure at low speeds to be extrapolated to zero airspeed with acceptable accuracy.

2. The propeller-plus-nacelle air loads have no effect on the extrapolation of zero-g air load to zero airspeed.

3. The propeller-plus-nacelle air load is a significant part of the unit additional air load (seven per cent of the shear), but not of the zero-g air load.

4. The effects of the flutter and rate of change of angle of attack are eliminated by averaging the increasing-g and decreasing-g data points.

5. Insufficient data are available to measure pitching acceleration, change in velocity during the maneuver, or propeller loads separate from nacelle loads. This investigation and unpublished work indicate the first two items have no effect on Lockheed C-130B. Propeller loads are calculated from wind tunnel data.

It is therefore concluded that the slope-intercept method as previously applied accounts for all variables that have significant effects on the total load. It can be applied to determine the distribution of load between the wing and attached power plants provided

sufficient data are available. The method has been used with some success on swept and straight wings, and on both subsonic and supersonic airplanes.

It is recommended that instrumentation be provided for the measurement of the airplane angle of attack, pitching acceleration, airspeed without lag, wing twist angles, and power effects independent of nacelle or other loads. The test program should include maneuvers at different weights, centers of gravity, and altitudes to provide data for the evaluation of these effects. Roller coasters should be performed with no power (and propellers feathered) applied by engines attached to the instrumented wing. The data should be investigated as done in this paper to determine the peculiarities of each type of airplane tested.

These conclusions and recommendations are those of the writer and are not necessarily those of the Lockheed-Georgia Company.

REFERENCES

1. Howland, W. L., and Buzzetti, C. J.: Measurements in Flight of Spanwise Wing Loading. Preprint No. 181, presented at Seventeenth Annual Meeting of the Institute of Aeronautical Sciences, January 24-27, 1954.

2. Skopinski, T. H., Aiken, W. S., Jr., and Huston, W. B.: Calibration of Strain-Gage Installations in Aircraft Structures for the Measurement of Flight Loads. National Advisory Committee on Aeronautics, TR 1178, 1954.

3. Gray, A. K.: Procedures Manual for Flight Test Determination and Evaluation of Load Distribution and Structural Integrity. Northrop Report EFT-55-1, June 1955.

4. Anonymous: Determination of Wing Bending Moment Distribution in Flight - F94B. Lockheed Aircraft Report LR-8489, October 1, 1952.

5. Aiken, W. S., Jr., and Howard, D. A.: A Comparison of Wing Loads Measured in Flight on a Fighter-Type Airplane by Strain-Gage and Pressure-Distribution Methods. NACA TN 1967, November 1949.

6. Flight Determination of Wing and Tail Loads on a Fighter-Type Airplane by Means of Strain-Gage Measurements. NACA TN 1729, 1948.

7. Rees, P. G.: Structural Demonstration of the C-130B Airplane. Lockheed Report ER-4061, February 16, 1960.

8. Bahr, W. C.: Engineering Flight Test Report of the Final Phase Combined Flight Load Survey and Structural Demonstration for the Model C-130A Airplane. Lockheed Report ER-2861, December 9, 1957.

9. Rees, P. G.: Results of the Initial Phase Structural Demonstration, Model C-130B Airplane. Lockheed Report ER-3926, August 4, 1959.

10. Stability and Control Section: Aerodynamic Data for Structural Design, C-130B. Lockheed Report ER-2899, June 1958.

11. McRae, D. D.: Weight, Balance and Moment of Inertia Calculations for Loads, Flutter and Dynamic Analysis. Lockheed Report ER-2434, April 10, 1958.

12. Dees, R. I.: Strain Gage Calibration for Loads Measurements on C-130A Aircraft - Ship 3011 - A. F. Serial No. 54-1624. Lockheed Report ER-2791, October 16, 1957.

13. Rumph, L. B., White, R. J., and Grumman, H. R.: Propeller Forces Due to Yaw and Their Effect on Airplane Stability. Journal of Aeronautical Sciences, October 1942, page 465.

14. Diehl, W. S.: Standard Atmosphere Tables and Data. NACA TR 218, 1948.

APPENDIX I

CURVES

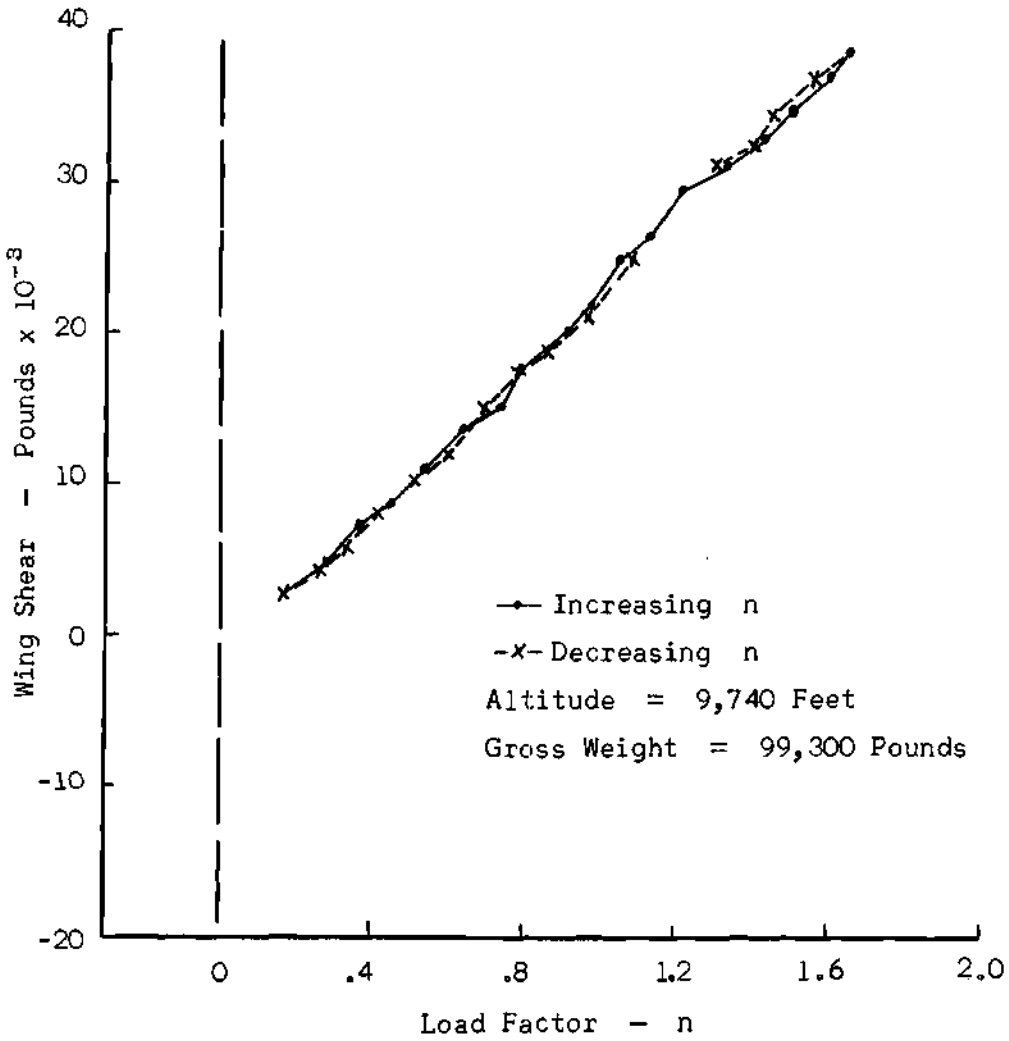

Figure 11. Shear at Wing Station 95 Versus Load Factor at a Dynamic Pressure of 387 Pounds per Square Foot

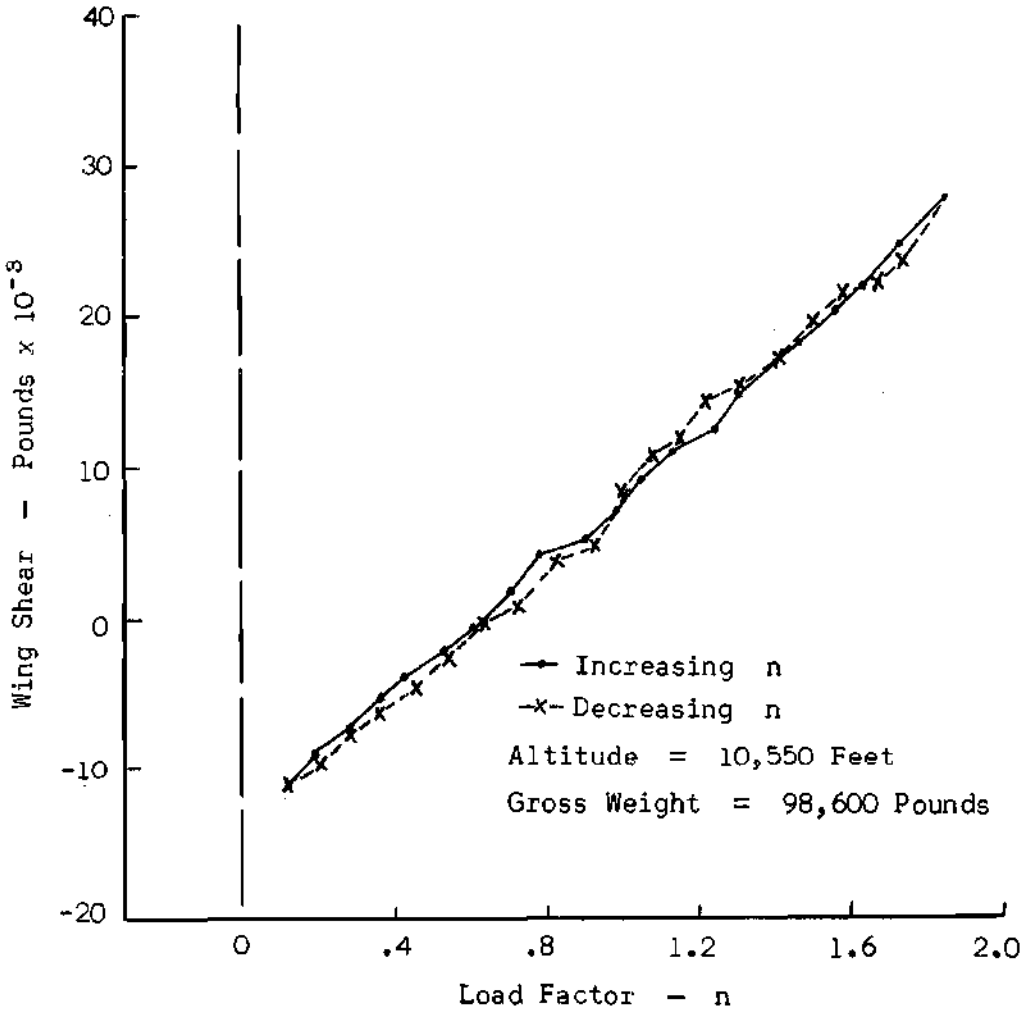

Figure 12. Shear at Wing Station 95 Versus Load Factor at a Dynamic Pressure of 69 Pounds per Square Foot

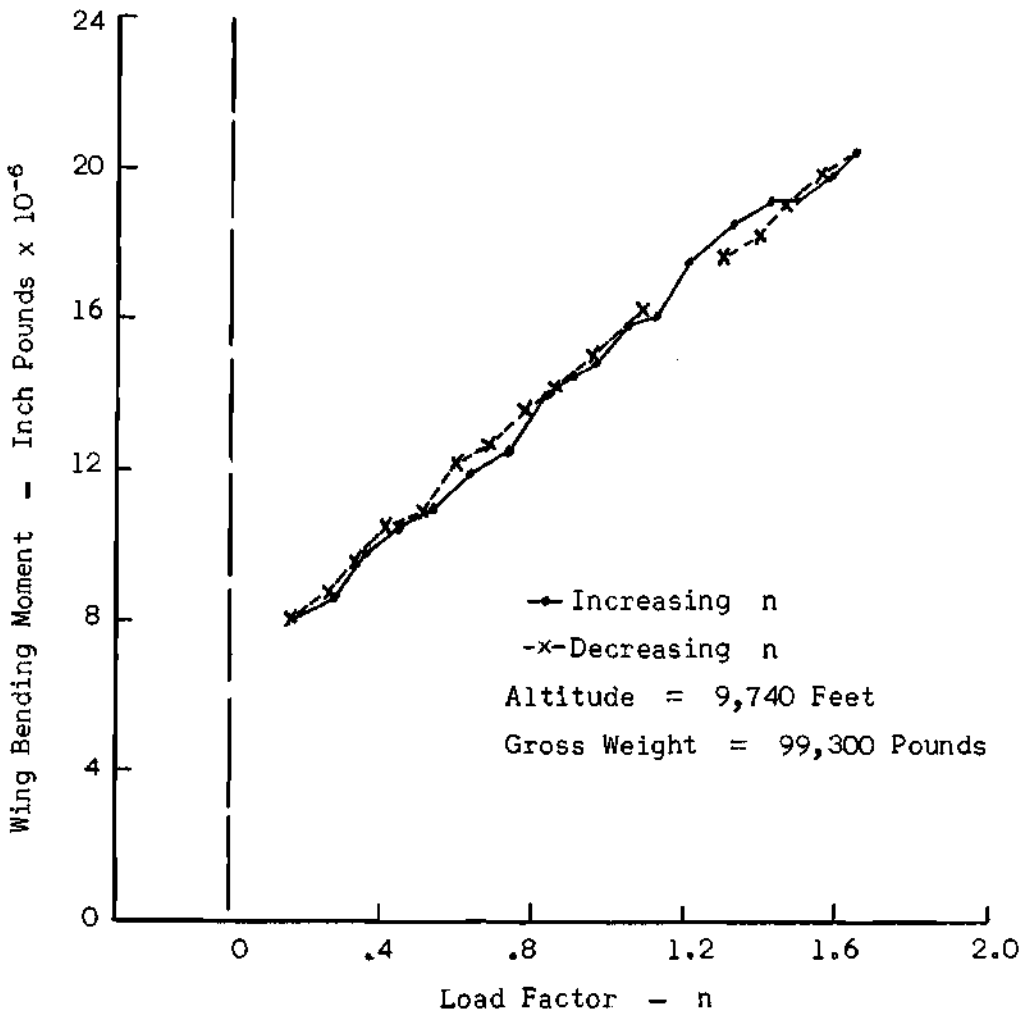

Figure 13. Bending Moment at Wing Station 95 Versus Load Factor at a Dynamic Pressure of 387 Pounds per Square Foot

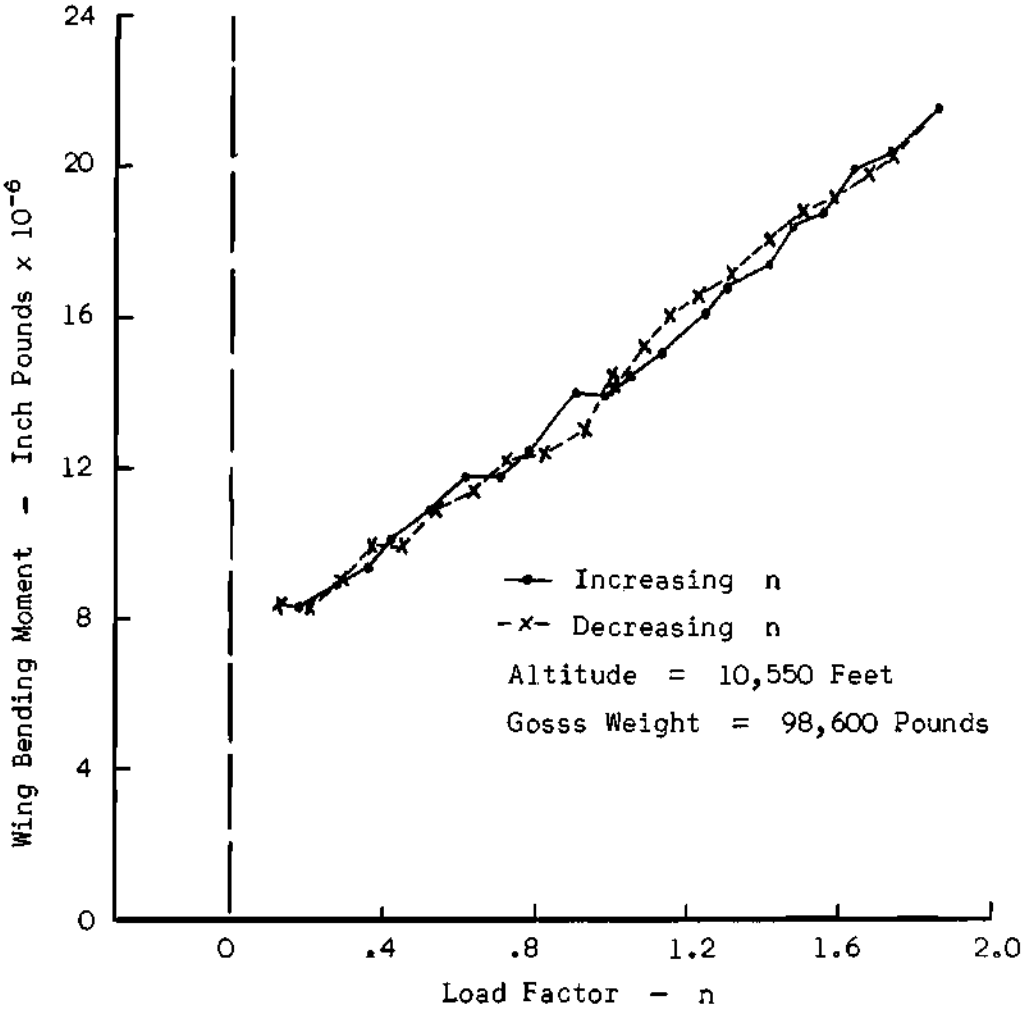

Figure 14. Bending Moment at Wing Station Versus Load Factor at a Dynamic Pressure of 69 Pounds per Square Foot

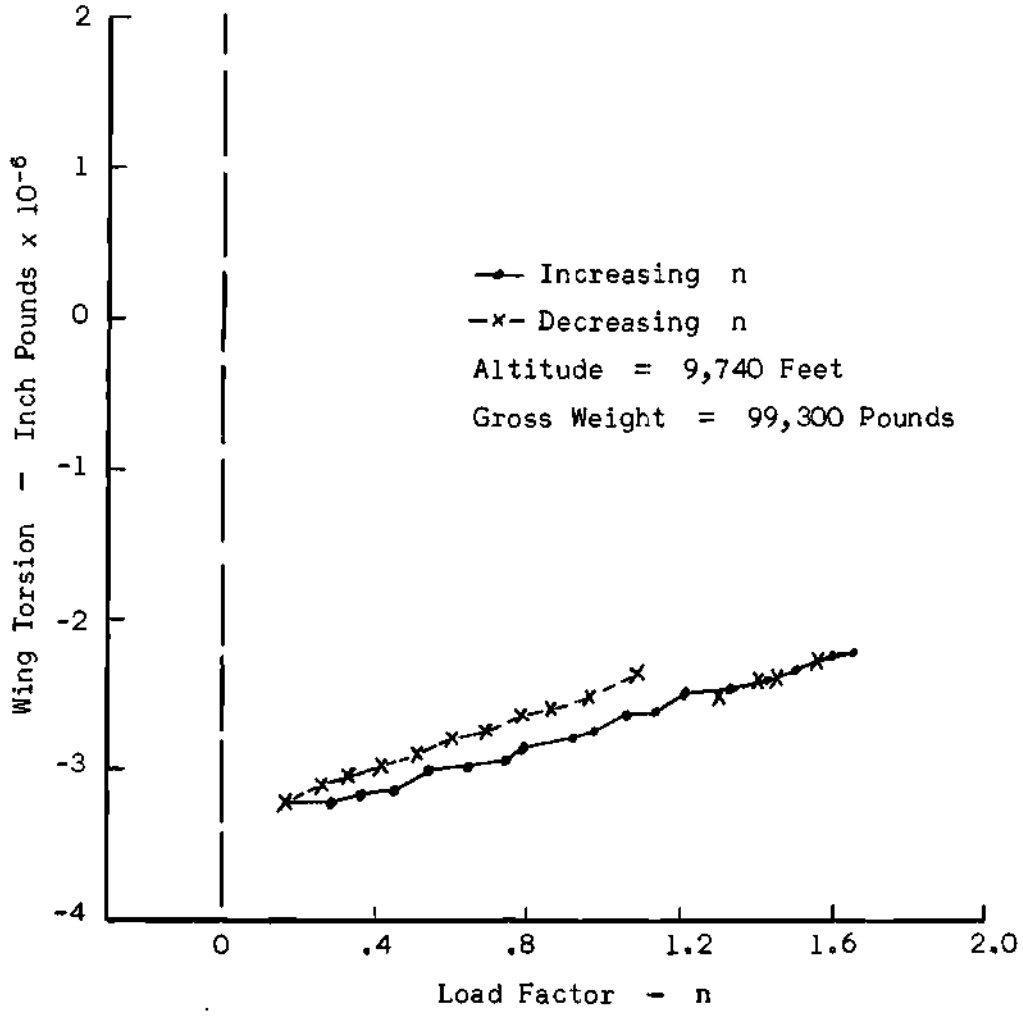

Figure 15. Torsion at Wing Station 95 Versus Load Factor at a Dynamic Pressure of 387 Pounds per Square Foot

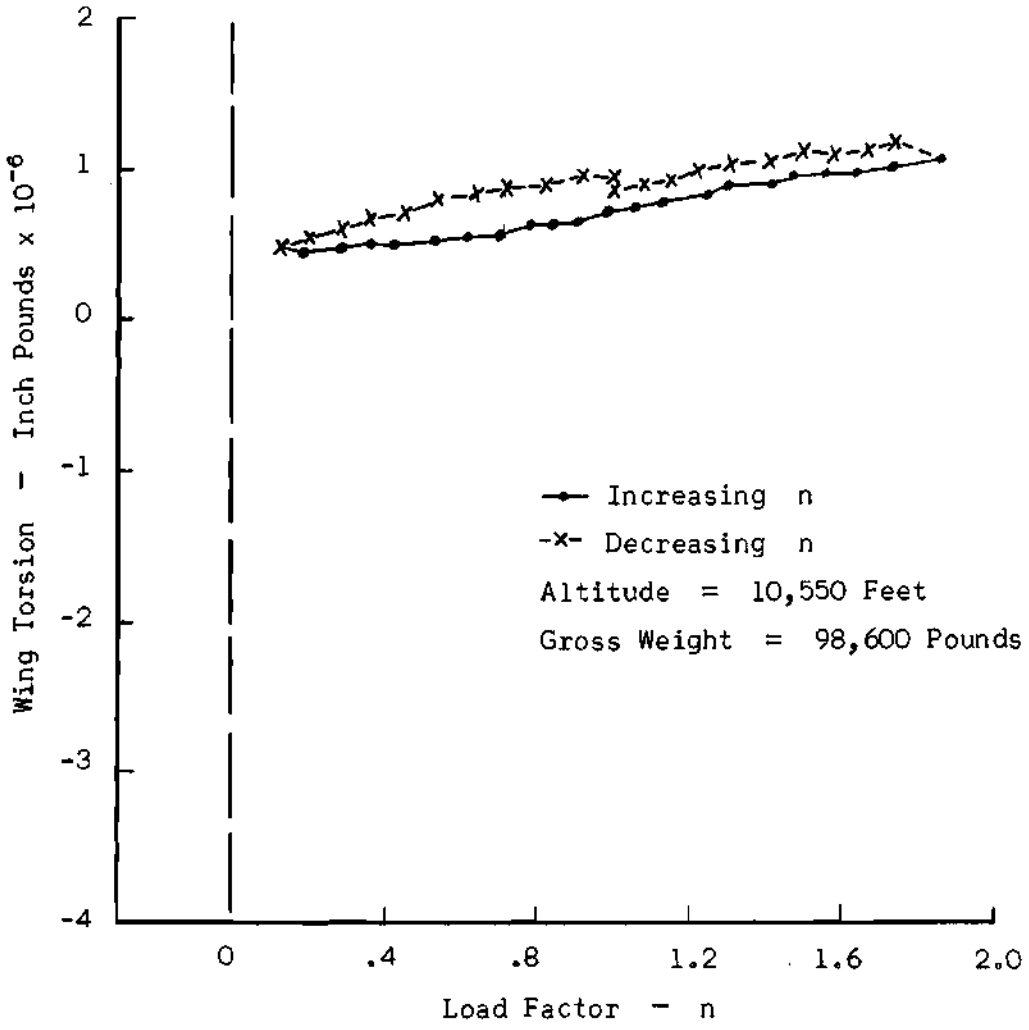

Figure 16. Torsion at Wing Station 95 Versus Load Factor at a Dynamic Pressure of 69 Pounds per Square Foot

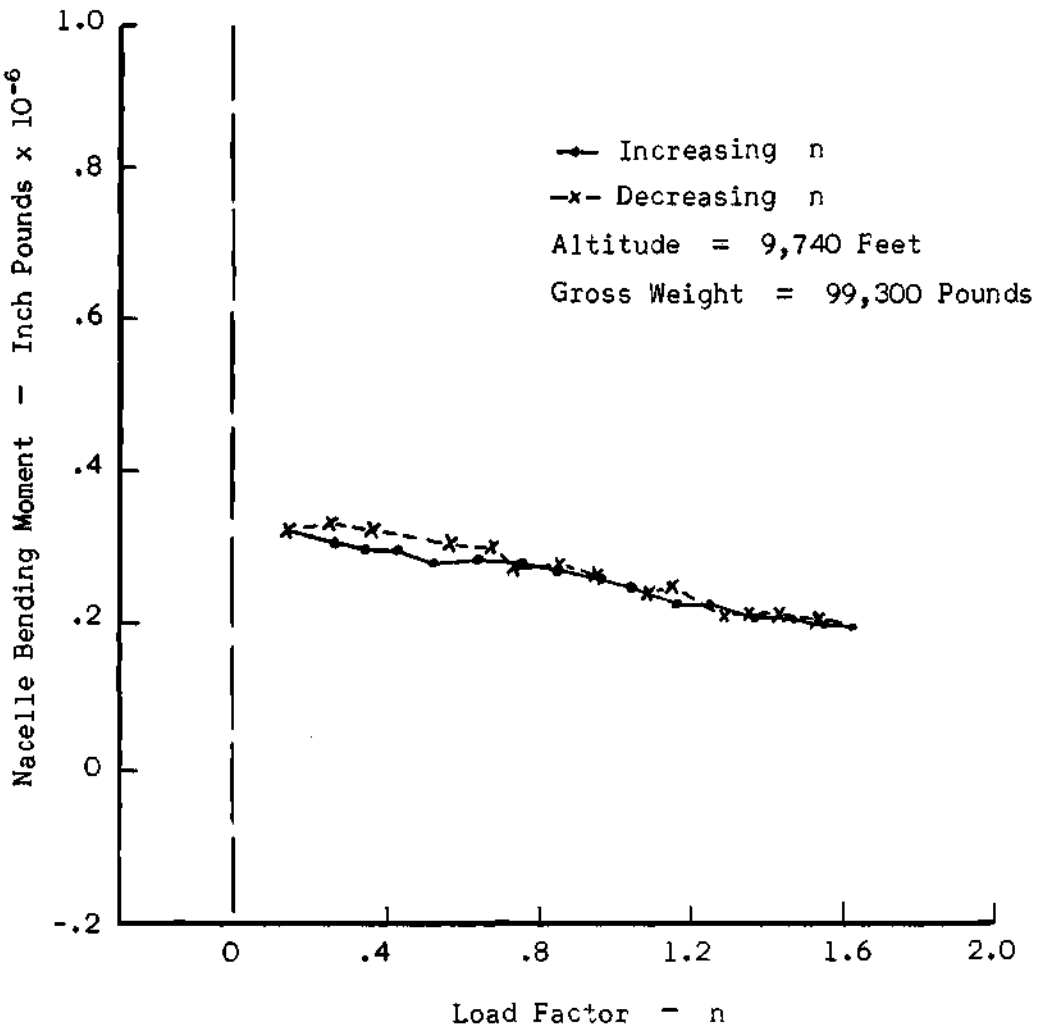

Figure 17. Nacelle Bending Moment Versus Load Factor at a Dynamic Pressure of 387 Pounds per Square Foot

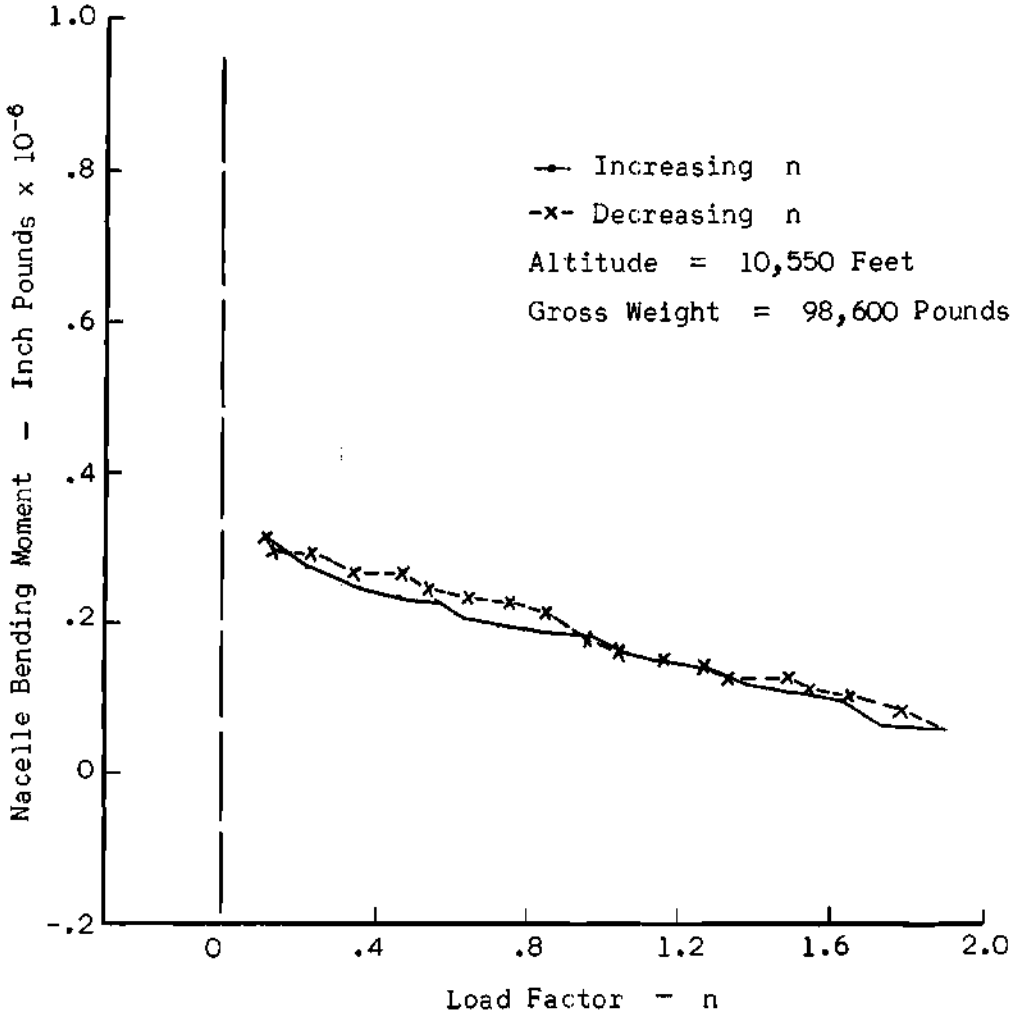

Figure 18. Nacelle Bending Moment Versus Load Factor of a Dynamic Pressure of 69 Pounds per Square Foot

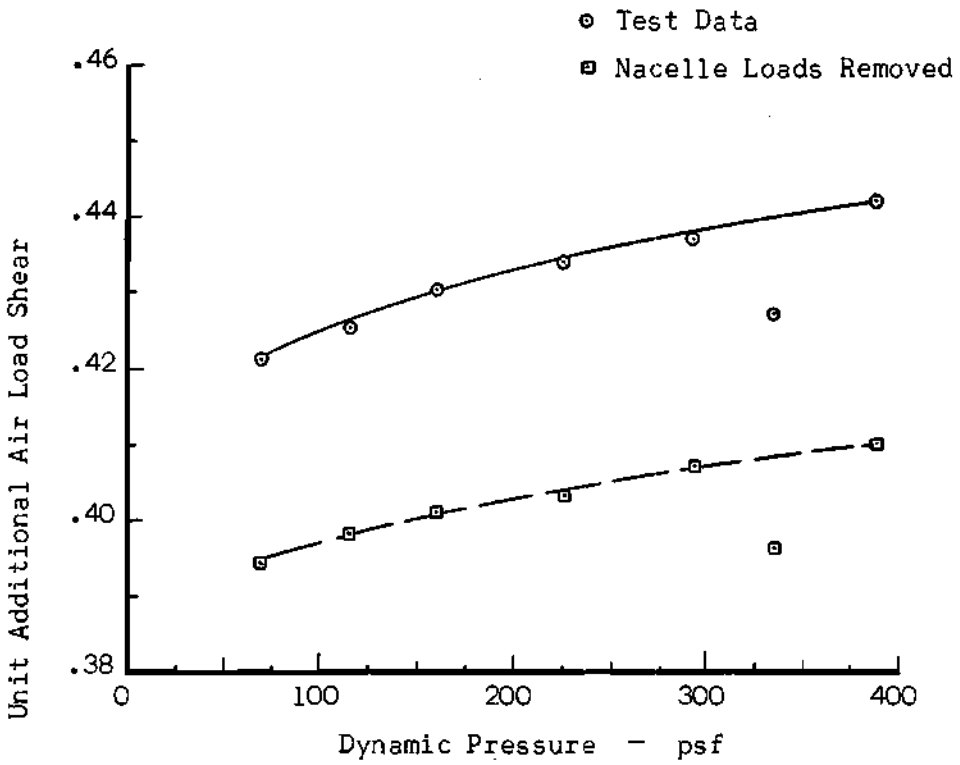

Figure 19. Wing Unit Additional Air Load Shear at Wing Station 95 Versus Dynamic Pressure

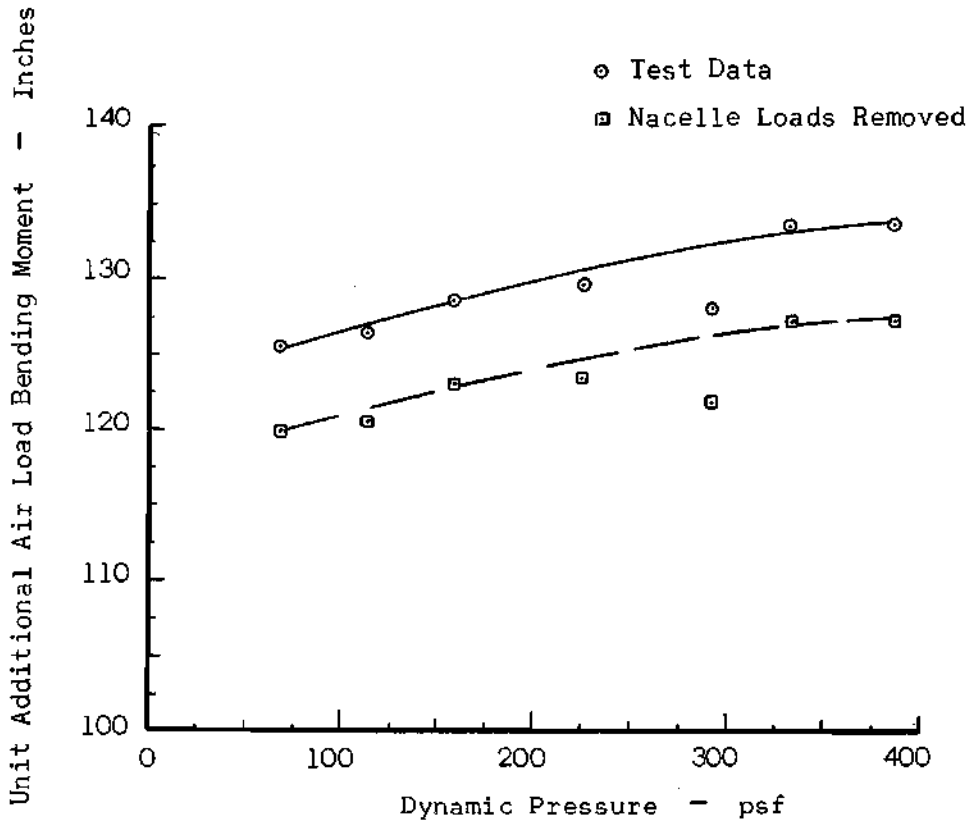

Figure 20. Wing Unit Additional Air Load Bending Moment at Wing Station 95 Versus Dynamic Pressure

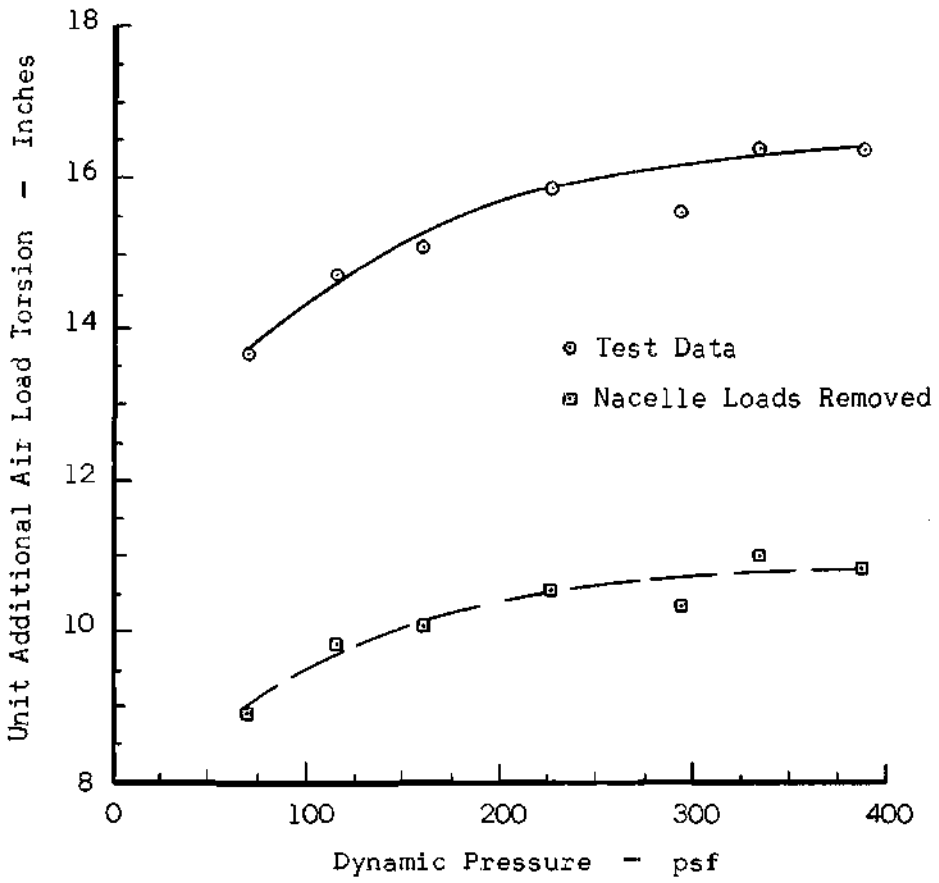

Figure 21. Wing Unit Additional Air Load Torsion at Wing Station 95 Versus Dynamic Pressure

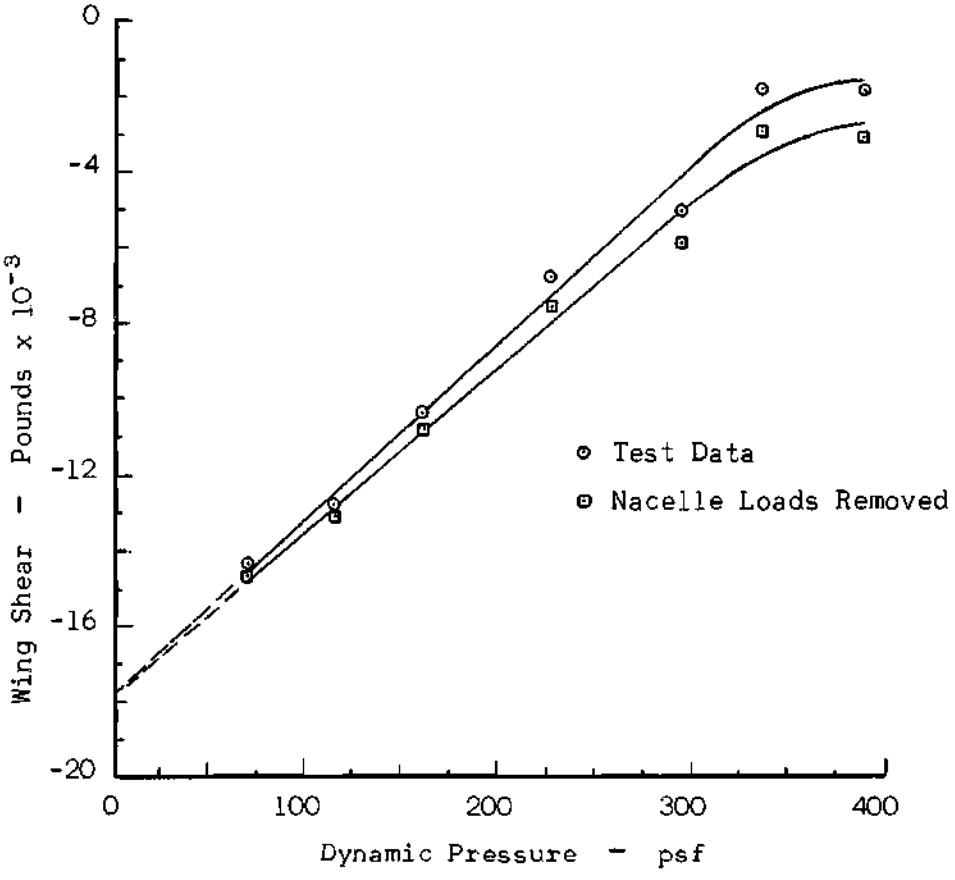

Figure 22. Wing Zero-g Air Load Shear at Wing Station 95 Versus Dynamic Pressure

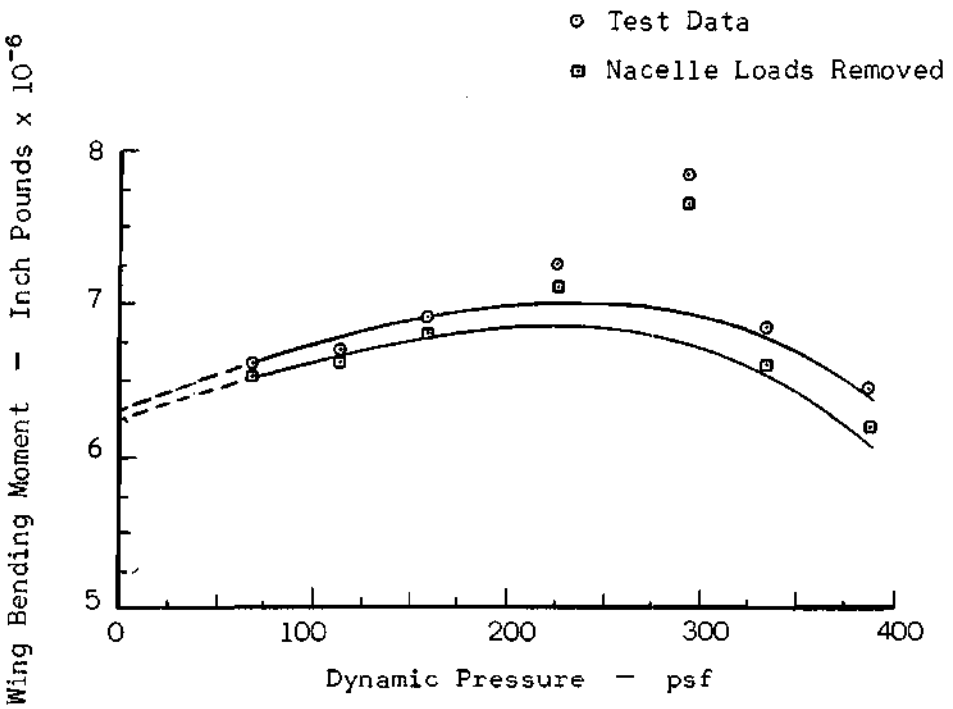

Figure 23. Wing Zero-g Air Load Bending Moment at Wing Station 95 Versus Dynamic Pressure

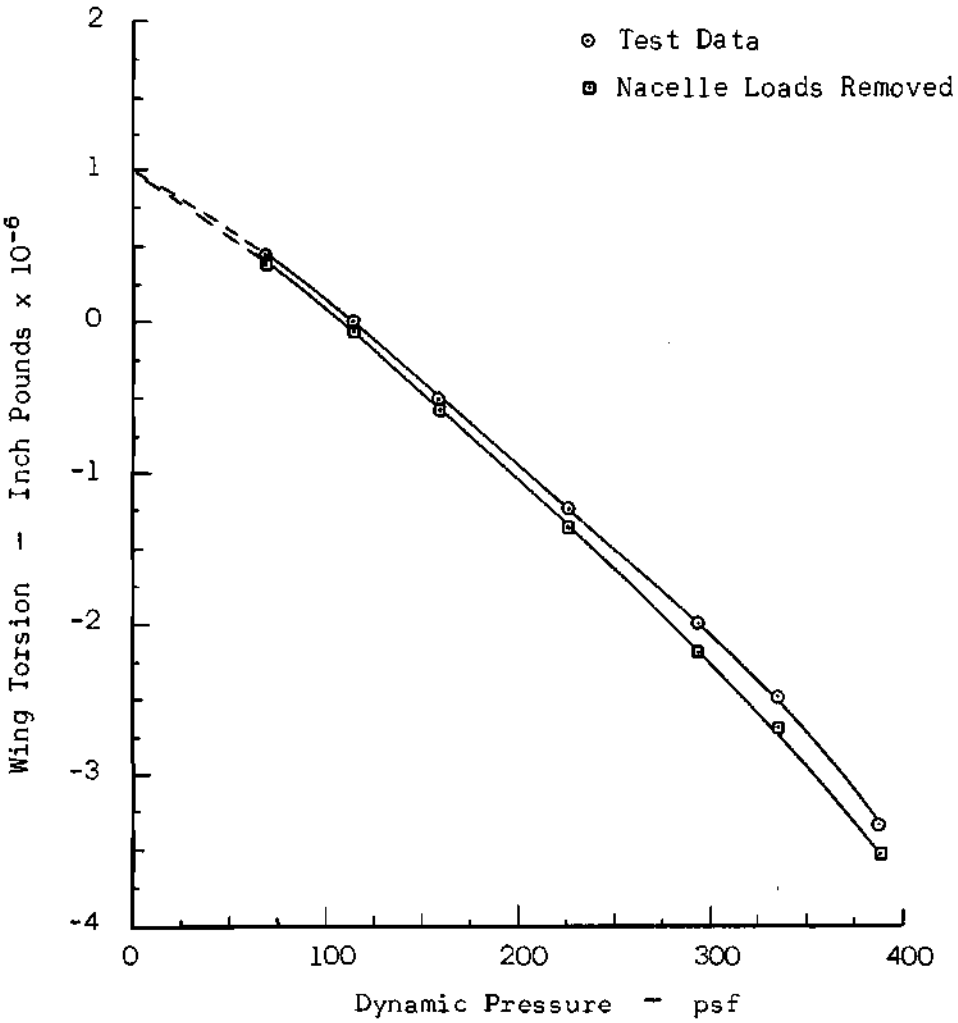

Figure 24. Wing Zero-g Air Load Torsion at Wing Station 95 Versus Dynamic Pressure

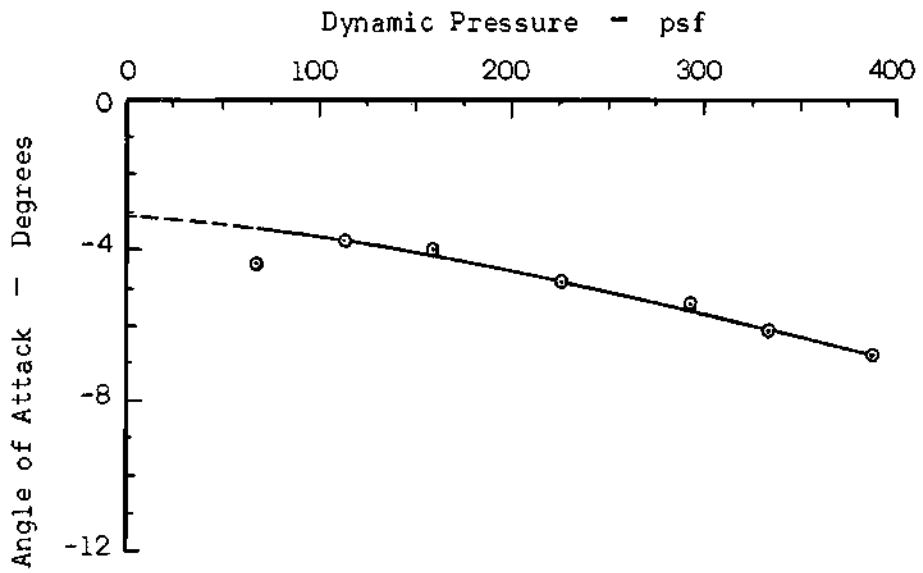

Figure 25. Wing Tip Angle of Attack at Zero Load Factor Versus Dynamic Pressure

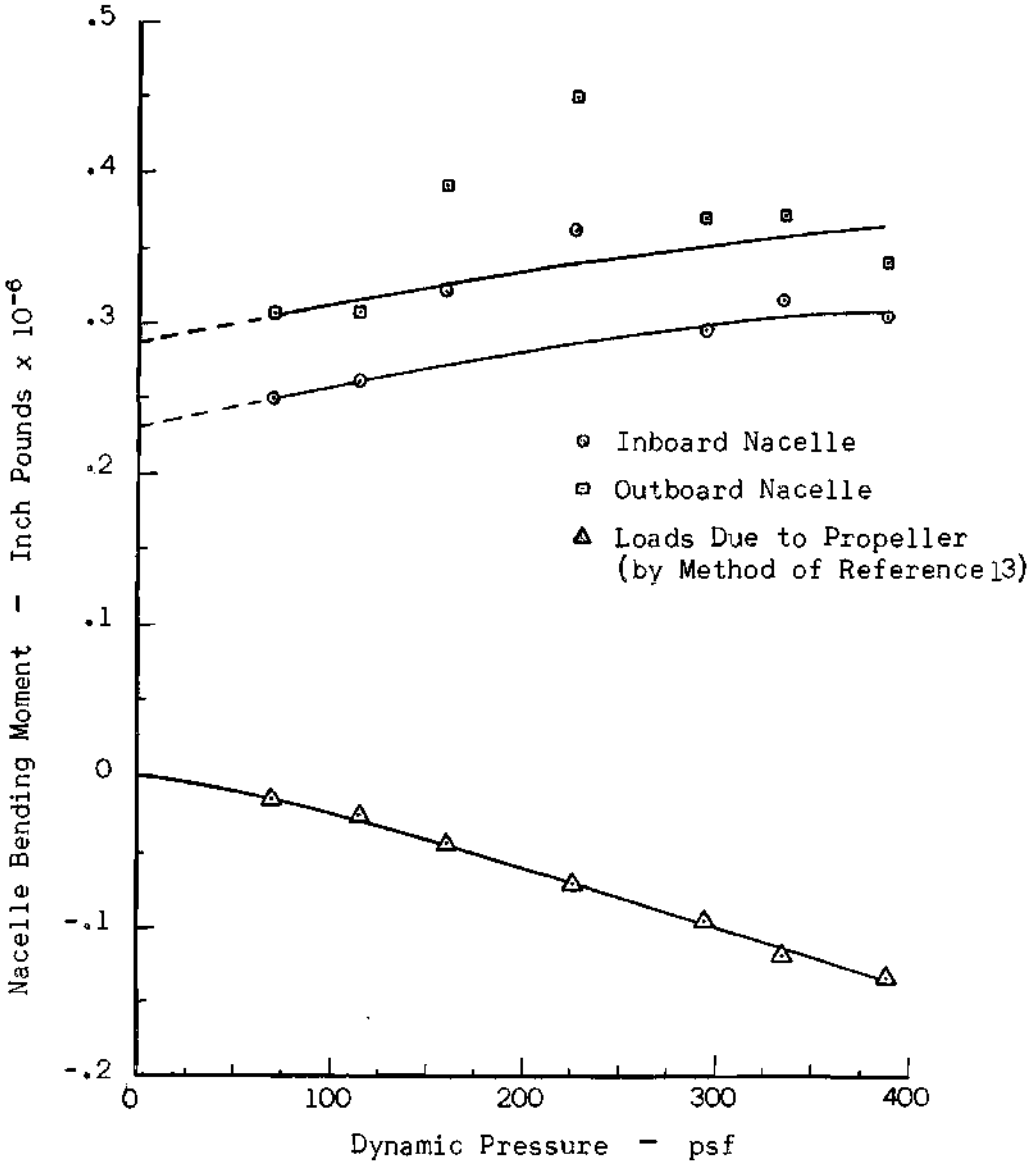

Figure 26. Nacelle Zero-g Air Load Bending Moment Versus Dynamic Pressure

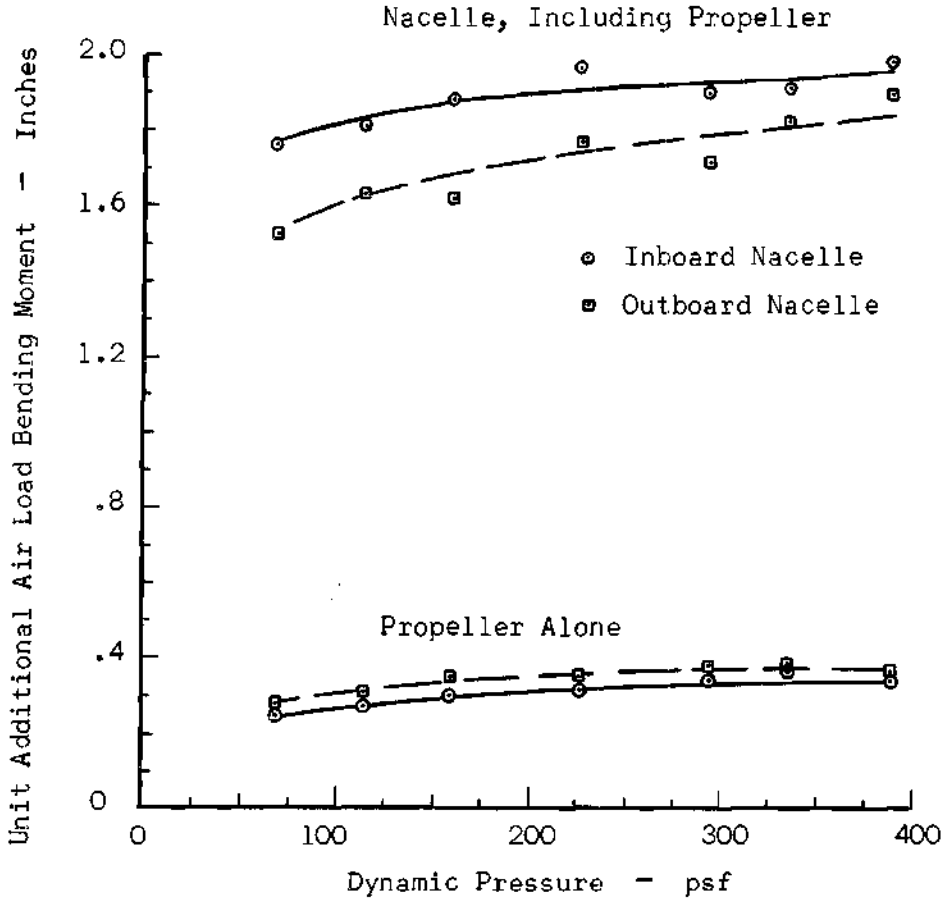

Figure 27. Nacelle Unit Additional Air Load Bending Moment Versus Dynamic Pressure

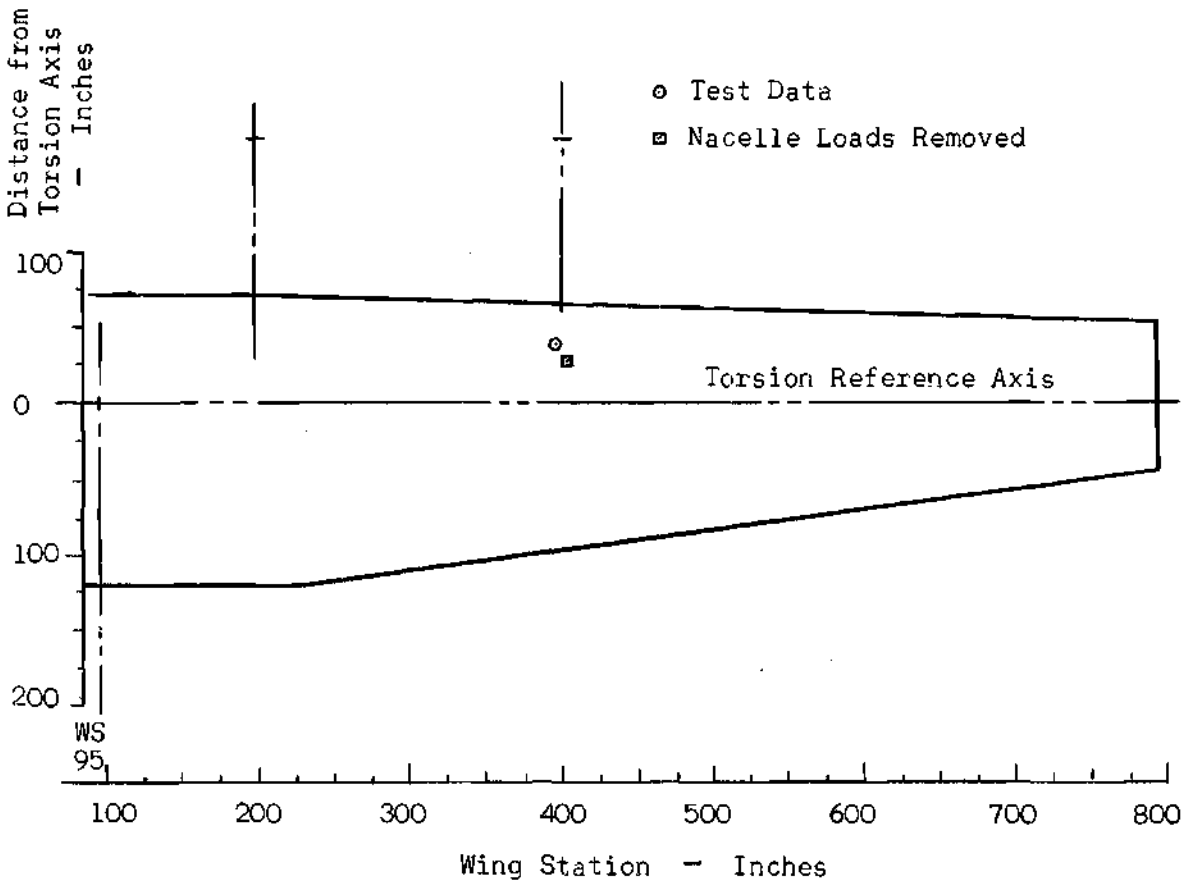

Figure 28. Center of Pressure of the Unit Additional Air Load Outboard of Wing Station 95 at a Dynamic Pressure of 387 Pounds per Square Foot

APPENDIX II

CALCULATIONS

Table 1. Load Factor and Other Parameters from Test Data

Run	Dynamic Pressure – PSF	Item	Units	Start of Maneuver	Δ Start to Min.	Min. n	Δ – Min. to Max.	Max. n	Δ – Max. to End	End of Roller Coaster
1	334	n		0.93		0.16		1.64		1.23
		α	Deg.	-3.5	-2.4	-5.9	3.5	-2.4	-1.1	-3.5
		t	Sec.	0	2.1	2.1	1.8	3.9	0.8	4.7
		Δα/Δt	Deg./Sec.		-1.14		1.95		-1.38	
2	387	n		1.08		0.16		1.65		1.30
		α	Deg.	-4.2	-2.0	-6.2	3.1	-3.1	-1.1	-4.2
		t	Sec.	0	2.6	2.6	2.0	4.6	0.9	5.5
		Δα/Δt	Deg./Sec.		-0.77		1.55		-1.22	
3	293	n		1.00		0.07		1.62		1.17
		α	Deg.	-3.1	-2.1	-5.2	3.5	-1.7	-1.1	-2.8
		t	Sec.	0	3.1	3.1	3.5	6.6	1.2	7.8
		Δα/Δt	Deg./Sec.		-0.68		1.00		-0.92	
4	226	n		0.96		0.03		1.90		1.17
		α	Deg.	-2.1	-2.7	-4.8	9.3	4.5	-6.2	-1.7
		t	Sec.	0	2.3	2.3→2.8	3.3	6.1	1.5	7.6
		Δα/Δt	Deg./Sec.		-1.18		2.82		-4.13	

Continued next page

Table 1 - continued

Run	Dynamic Pressure – PSF	Item	Units	Start of Manuever	Δ Start to Min.	Min. n	Δ – Min. to Max.	Max. n	Δ – Max. to End	End of Roller Coaster
5	158	n		0.99		-0.10		1.94		0.98
		α	Deg.	-0.3	-4.2	-4.5	8.7	4.2	-4.5	-0.3
		t	Sec.	0	3.0	3.0	3.9	6.9	1.7	8.6
		Δα/Δt	Deg./Sec.		-1.40		2.23		-2.64	
6	114	n		1.00		0		1.91		1.08
		α	Deg.	2.4	-6.2	-3.8	11.8	8.0	-5.6	2.4
		t	Sec.	0	2.8	2.8→3.1	4.0	7.1	1.5	8.6
		Δα/Δt	Deg./Sec.		-2.22		2.95		-3.74	
7	69	n		1.00		0.12		1.86		1.00
		α	Deg.	3.8	-6.9	-3.1	17.3	14.2	-8.3	5.9
		t	Sec.	0	2.2	2.2→2.7	5.2	7.9	2.2	10.1
		Δα/Δt	Deg./Sec.		-3.14		3.33		-3.77	

Calculation of Constants for Table 2

$$J = \frac{V_T}{nD}$$

$$n = 17.08 \text{ rps}$$

$$D = 13.5 \text{ ft.}$$

$$V_{fps} = \frac{6080}{3600} = 1.689\ V_{KTS}$$

$$J = \frac{1.689\ V_T(KTS)}{17.08 \times 13.5} = 0.00735\ V_T(KTS)$$

Propeller Shaft Horsepower

$$SHP = \frac{\text{Torque (in. lb.)} \times \text{Shaft Radians/Sec.}}{12 \times 550} - 60$$

$$= \frac{T \times \frac{13{,}820}{60} \times 2\pi}{12 \times 550} - 60$$

$$= 0.219\ T - 60 \quad \text{(HP)}$$

Torque is measured on the engine shaft where the speed is 13,820 rpm.

Arbitrary loss in reduction gears = 60 HP.

$$C_P = \frac{SHP \times 550}{\rho_o \sigma\ n^3 D^5} = \frac{SHP \times 550}{\sigma \cdot 0.002378 \times \left(\frac{17.08}{10}\right)^3 (13.5)^5} = 0.105\ \frac{SHP}{\sigma}$$

$$F_P = C_T\ \rho_o \sigma\ n^2 D^4 = 0.002378 \times (17.08)^2 (13.5)^4\ \sigma C_T = 22{,}799\ \sigma C_T$$

$$T_{HP} = \frac{F_P(lb.) \times V_T(FPS)}{550} = \frac{F_P \times 1.689\ V_T(KTS)}{550} = \frac{F_P(lb.) \times V_T(KTS)}{325}$$

$$q = \frac{\rho}{2} V_{FPS}^2 = \frac{.002378}{2} (1.689\ V_{e_{KTS}})^2 = \frac{V_{e_{KTS}}^2}{295}$$

Propeller Normal Force per Radian

$$\frac{P_z}{\alpha} = \frac{C_z}{\alpha} \cdot qS = R_1 \frac{D^2}{S} \cdot qS$$

$$= 182\, R_1 q$$

where $D = 13.5$ ft., $D^2 = 182$

Nacelle Load from $\frac{P_z}{\alpha}$:

$$\frac{M_{Y_{NAC}}}{\alpha} = 120 \cdot \frac{P_z}{\alpha}$$

$$= 21{,}840\, R_1 q \quad \text{(in. lb./Rad.)}$$

where moment arm from propeller axis to average nacelle strain gage station = 120 in.

Proller Pitching Moment per Radian per Second

$$\frac{M_Y}{\dot{\theta}} = \frac{C_m}{\dot{\theta}} \cdot q\, S\bar{c}$$

$$= \frac{R_4 D^4 \cdot q\, S\bar{c} \times 12}{2\, S\bar{c}\, V_T(\text{fps})}, \qquad D = 13.5$$

$$= \frac{R_4 D^4\, q \times 12}{2 V_T} \qquad D^4 = 33{,}250$$

$$= \frac{33{,}250\, R_4 q \times 12}{2 \times 1.689\, V_T(\text{knots})}, \qquad 1 \text{ Knot} = 1.689 \text{ fps}$$

$$= 118{,}200 \frac{R_4 q}{V_T(\text{knots})} \qquad \text{(in. lb. sec.)}$$

$$T_c = \frac{F_P}{\rho V^2 D^2}$$

Table 2. Calculation of Propeller Parameters

1	2	3	4	5	6	7	8	9	10	11	12	13	14
Run	Engine	Torque	Alt.	FAT	$\sigma^{\frac{1}{2}}$	V_e	V_T	J	Prop. SHP	C_P	C_T	F_P	THP
		in.lb.		Deg.C	Ref.14	Test Data	Kts ⑦*/⑥	.00737 ⑧	.219 ③ - 60	.105 ⑩ / ⑥²	Test Data	lb. ⑫ ⑥² x 22,799	⑬ ⑧ / 325
		----------Test Data----------											
1	3	15,900	12,100	17	0.7936	314	396	2.91	3,422	.571	.173	2,484	3,027
	4	15,450	12,100	17	0.7936	314	396	2.91	3,324	.554	.168	2,412	2,940
2	3	17,250	9,740	21	0.8252	338	410	3.02	3,718	.573	.166	2,577	3,251
	4	17,200	9,740	21	0.8252	338	410	3.02	3,707	.572	.165	2,562	3,232
3	3	11,700	10,030	17	0.8262	294	356	2.62	2,502	.385	.132	2,054	2,250
	4	11,500	10,030	17	0.8262	294	356	2.62	2,458	.378	.130	2,023	2,216
4	3	14,200	9,870	13	0.8343	258	309	2.27	3,050	.460	.176	2,793	2,656
	4	14,350	9,870	13	0.8343	258	309	2.27	3,083	.465	.185	2,936	2,791
5	3	7,000	10,640	10	0.8262	216	261	1.92	1,473	.227	.104	1,619	1,300
	4	6,900	10,640	10	0.8262	216	261	1.92	1,451	.223	.102	1,587	1,274
6	3	4,150	10,780	8	0.8258	183	222	1.63	849	.131	.063	979	669
	4	4,000	10,780	8	0.8258	183	222	1.63	816	.126	.060	933	637
7	3	2,700	10,550	6	0.8338	143	172	1.26	531	.080	.043	682	300
	4	2,700	10,550	6	0.8338	143	172	1.26	531	.080	.043	682	300

*Numbers in circles refer to column numbers

Continued next page

Table 2 (Continued)

1	2	15	16	17	18	19	20	21	22	23	24	25
Run	Engine	M_1	M_2	N_1	N_2	R_1	R_4	q	P_z/α	M_{500}/α from P_z/α	$M_{\dot{\gamma}}/\dot{\theta}$ Prop.	T_c
----------Reference 13----------						(12)x(15) +4 x(16)	(11)x(17) -4 x(18)	PSF (7)^2/295	lb./rad. 182 (19)(21)	in.lb. x 10^6 per rad. 120 (22)	in.lb./rad. per sec. 118,200 (20) x (21)/(8)	.002747 (13)/(21)
1	3	.072	.072	.0066	.013	.310	-.0482	334	18,800	2.26	-4810	.0204
	4	.072	.072	.0066	.013	.309	-.0484	334	18,780	2.25	-4820	.0198
2	3	.072	.073	.0055	.0135	.304	-.0508	387	21,400	2.57	-5660	.0183
	4	.072	.073	.0055	.0135	.304	-.0509	387	21,400	2.57	-5670	.0182
3	3	.082	.069	.0080	.0102	.287	-.0377	293	15,300	1.836	-2790	.0193
	4	.082	.069	.0080	.0102	.287	-.0378	293	15,300	1.836	-2790	.0190
4	3	.100	.0645	.0115	.008	.276	-.027	226	11,330	1.36	-2390	.0340
	4	.100	.0645	.0115	.008	.276	-.027	226	11,330	1.36	-2390	.0356
5	3	.117	.0595	.0150	.007	.250	-.025	158	7,200	.864	-1790	.0282
	4	.117	.0595	.0150	.007	.250	-.025	158	7,200	.864	-1790	.0276
6	3	.124	.0535	.019	.006	.222	-.022	114	4,600	.552	-1340	.0236
	4	.124	.0535	.019	.006	.221	-.022	114	4,600	.552	-1340	.0224
7	3	.15	.046	.026	.005	.190	-.018	69	2,390	.287	- 855	.0272
	4	.15	.046	.026	.005	.190	-.018	69	2,390	.287	- 855	.0272

$.002747 = 1/(2D^2) = 1/(2 \times 182)$

Table 3. Calculation of Angles and Rates

Run	V_T	q	Gross Weight	$C_{L_{n=1}}$	$\Delta\alpha_{\Delta n=1}$	Avg. $\dot{\alpha}/g$ Deg./Sec./g	$\Delta\alpha/\Delta nW$	$\gamma/\Delta n$ Rad./Sec./g	$\dot{\theta}$ Deg./ Sec./g
	Kts	Psf	Lb.	.00573 ④/③	Deg. ⑤ /0.096	Table 1	Deg. x 10^6 Lb. ⑥/④	19.07/②	57.3 ⑨ + ⑧
1	396	334	99,400	0.170	1.75	-1.14	1.76	.0482	4.52
2	410	387	99,300	0.147	1.51	-0.77	1.52	.0465	4.18
3	356	293	98,950	0.193	1.99	-0.68	2.01	.0536	5.08
4	309	226	98,800	0.251	2.60	-1.18	2.63	.0617	6.17
5	261	158	98,750	0.358	3.70	-1.40	3.75	.0731	7.94
6	222	114	98,700	0.496	5.15	-2.22	5.22	.0860	10.15
7	172	69	98,600	0.82	8.45	-3.14	8.58	.1110	14.94

$.000573 = 1/1745 - 1/S_w$ $\quad$ $19.07 = 32.2/1.689 \rightarrow$ Conversion Factor FPS to Knots

Table 4. Propeller and Nacelle Basic and Unit Additional Air Load

1	2	3	4	5	6	7	8	9	10	11	12	13
Run	Prop.	P_z/α	M_Y/α	$\Delta\alpha/nW$	$M_Y/\dot{\alpha}$	$\dot{\alpha}_{n=o}$	$P_{z_{n=o}}$	$M_{Y_{n=o}}$	P_z/nW	M_Y/nW	Test Values $M_{Y_{n=o}}$	Test Values M_Y/nW
		Lb./Rad.	x 10^{-6} In. Lb./Rad.	Rad. x 10^6	In.Lb./Rad./Sec.	Rad./Sec.	③$\alpha_{n=o}$	④$\alpha_{n=o}$	x 10^{-3} ③ ⑤	④ ⑤	In.Lb. x 10^{-6}	In.
1	3	18,800	2.26	.307	-4810	-.020	978	-.117	.00577	.695	.315	1.91
	4	18,780	2.25	.307	-4820	-.020	976	-.117	.00576	.690	.371	1.83
2	3	21,400	2.57	.266	-5660	-.013	1113	-.134	.00570	.685	.305	1.99
	4	21,400	2.57	.266	-5670	-.013	1113	-.134	.00570	.685	.339	1.90
3	3	15,300	1.84	.351	-2790	-.012	795	-.096	.00536	.645	.294	1.90
	4	15,300	1.84	.351	-2790	-.012	795	-.096	.00536	.645	.369	1.71
4	3	11,330	1.36	.459	-2390	-.021	590	-.071	.00519	.624	.362	1.97
	4	11,330	1.36	.459	-2390	-.021	590	-.071	.00519	.624	.450	1.77
5	3	7,200	.86	.655	-1790	-.025	374	-.045	.00471	.563	.319	1.88
	4	7,200	.86	.655	-1790	-.025	374	-.045	.00471	.563	.391	1.62
6	3	4,600	.55	.91	-1340	-.039	239	-.029	.00419	.500	.259	1.81
	4	4,600	.55	.91	-1340	-.039	239	-.029	.00419	.500	.308	1.63
7	3	2,390	.29	1.50	- 855	-.055	124	-.015	.00358	.435	.248	1.76
	4	2,390	.29	1.50	- 855	-.055	124	-.015	.00358	.435	.307	1.53

$\alpha_{n=o}$ = -3.00°= -.052 Rad.